Response of the Ocean Natural Carbon Storage to Projected Twenty-First-Century Climate Change

RAFFAELE BERNARDELLO AND IRINA MARINOV

Department of Earth and Environmental Science, The University of Pennsylvania, Philadelphia, Pennsylvania

JAIME B. PALTER

Department of Atmospheric and Oceanic Sciences, McGill University, Montreal, Quebec, Canada

JORGE L. SARMIENTO

Atmospheric and Oceanic Sciences Program, Princeton University, Princeton, New Jersey

ERIC D. GALBRAITH

Department of Earth and Planetary Sciences, McGill University, Montreal, Quebec, Canada

RICHARD D. SLATER

Atmospheric and Oceanic Sciences Program, Princeton University, Princeton, New Jersey

(Manuscript received 15 June 2013, in final form 5 November 2013)

ABSTRACT

The separate impacts of wind stress, buoyancy fluxes, and CO_2 solubility on the oceanic storage of natural carbon are assessed in an ensemble of twentieth- to twenty-first-century simulations, using a coupled atmosphere–ocean–carbon cycle model. Time-varying perturbations for surface wind stress, temperature, and salinity are calculated from the difference between climate change and preindustrial control simulations, and are imposed on the ocean in separate simulations. The response of the natural carbon storage to each perturbation is assessed with novel prognostic biogeochemical tracers, which can explicitly decompose dissolved inorganic carbon into biological, preformed, equilibrium, and disequilibrium components. Strong responses of these components to changes in buoyancy and winds are seen at high latitudes, reflecting the critical role of intermediate and deep waters. Overall, circulation-driven changes in carbon storage are mainly due to changes in buoyancy fluxes, with wind-driven changes playing an opposite but smaller role. Results suggest that climate-driven perturbations to the ocean natural carbon cycle will contribute 20 Pg C to the reduction of the ocean accumulated total carbon uptake over the period 1860–2100. This reflects a strong compensation between a buildup of remineralized organic matter associated with reduced deep-water formation (+96 Pg C) and a decrease of preformed carbon (−116 Pg C). The latter is due to a warming-induced decrease in CO_2 solubility (−52 Pg C) and a circulation-induced decrease in disequilibrium carbon storage (−64 Pg C). Climate change gives rise to a large spatial redistribution of ocean carbon, with increasing concentrations at high latitudes and stronger vertical gradients at low latitudes.

1. Introduction

Carbon dioxide concentrations in the modern atmosphere are governed by the difference between anthropogenic emissions and uptake by the ocean and the terrestrial biosphere. The ocean has been a net sink of anthropogenic CO_2 over the last 200 years, removing more than 30% of anthropogenic carbon emitted to the atmosphere (Sabine et al. 2004). Importantly, since the beginning of the industrial revolution, the ocean carbon cycle can be described as the sum of the natural carbon cycle, which was in a balanced state in preindustrial times, plus an anthropogenic perturbation. The latter includes two interconnected components: 1) the addition of CO_2 to the atmosphere, and hence to the ocean, and 2) a climate

Corresponding author address: Raffaele Bernardello, Earth and Environmental Science, The University of Pennsylvania, Hayden Hall, 240 S. 33rd St., Philadelphia, PA 19104-6316.
E-mail: braf@sas.upenn.edu

DOI: 10.1175/JCLI-D-13-00343.1

change component. The second component can affect the ability of the ocean to absorb anthropogenic CO_2 but also the ocean natural carbon cycle. This study focuses on this last aspect by looking at the mechanisms through which climate change can alter the preindustrial natural carbon cycle of the ocean. In doing this we deliberately ignore the uptake of anthropogenic CO_2 that results from the increase of atmospheric CO_2 and focus only on the response of the background natural carbon cycle to climate change.

Carbon is stored in the ocean interior because of its high solubility in cold polar waters and its continuous transfer from the surface ocean to depth by the vertical flux of organic carbon, the ''biological pump'' (Volk and Hoffert 1985). Ocean carbon storage, particularly the biological pump, plays a critical role in climate by regulating atmospheric pCO_2 values (Sarmiento and Toggweiler 1984; Marinov et al. 2006). In the absence of the biological pump, atmospheric pCO_2 would be about 140 ppm higher (Gruber and Sarmiento 2002). Paleoclimatologists have often invoked changes in the biological pump to explain large glacial/interglacial variations of atmospheric pCO_2 (Sigman and Boyle 2000; Sigman et al. 2010). By contrast, the role of ocean carbon storage in transient, decadal-scale climate change has been less explored and is not well understood.

The processes regulating ocean carbon storage are tightly interconnected and include atmosphere–ocean gas exchange, photosynthesis, remineralization, mixing, and transport. Many of these processes are expected to change in a warming climate. Changes in heat and freshwater fluxes are expected to increase upper ocean stratification (Durack and Wijffels 2010; Capotondi et al. 2012), requiring more energy to initiate vertical mixing and possibly leading to weaker exchange between the surface and deep ocean. Warming will directly reduce CO_2 solubility of the surface waters, with important feedbacks for atmospheric pCO_2 (Archer et al. 2004; Goodwin and Lenton 2009). A combination of rising greenhouse gas concentrations and ozone depletion has changed atmospheric temperature and pressure patterns, strengthening midlatitude westerly winds belts and shifting them poleward (Thompson and Solomon 2002; Strong and Davis 2007). The stronger winds at high latitudes provide more energy for the mechanical mixing of the water column and can alter buoyancy budgets in the formation regions of various mode, intermediate, and deep-water masses. The effect of a stronger mechanical mixing on carbon storage is the subject of great debate, especially in the Southern Ocean where the observed intensification of the westerlies over the past 50 years has possibly weakened the net ocean CO_2 sink already (Le Quéré et al. 2007; Law et al. 2008; Zickfeld et al. 2008). The wind-driven upwelling of carbon-rich Circumpolar Deep Waters (CDW) plays an important role in determining the strength of the total CO_2 sink (Lenton and Matear 2007; Lovenduski et al. 2008; Le Quéré et al. 2010). The gradual ozone recovery over the twenty-first century is poised to counteract the increasing greenhouse gas concentrations, with uncertain results for the westerly winds in the Southern Hemisphere (Son et al. 2009; Karpechko et al. 2010; Arblaster et al. 2011; Polvani et al. 2011; Simpkins and Karpechko 2012).

The goal of this paper is to separately assess the impacts of changes in wind stress, buoyancy fluxes, and CO_2 solubility on the oceanic distribution and storage of natural carbon in an ensemble of twentieth- to twenty-first-century simulations using a coupled atmosphere–ocean climate model. One of our hypotheses at the outset of this work was that changes in wind stress over this period would oppose changes in buoyancy fluxes, counterbalancing to some degree the impact on total carbon uptake (e.g., Matear and Lenton 2008). However, any change in ocean circulation influences a tangled web of processes in the ocean's carbon system, with some processes favoring increased ocean carbon storage and others leading to decline. For instance, a projected reduction in deep-water mass formation rates would slow the transport of cold carbon-rich water to depth, reducing the ocean's capacity to store carbon. On the other hand, a lengthening of residence time of water at depth allows an increase in the accumulation of carbon coming from the remineralization of sinking organic particles (Marinov et al. 2008b; Kwon et al. 2011). The net effect on ocean carbon storage is far from obvious.

We propose that a thorough accounting of each process is the only path toward a mechanistic understanding of these controls. To this end, we use a coupled atmosphere–ocean model with a newly developed ocean biogeochemical model that includes a prognostic partitioning of biogeochemical tracers. This allows the explicit separation of a tracer into its preformed concentration (the concentration a parcel of water had the last time it was at the ocean surface) and its regenerated concentration (the concentration resulting from biological remineralization in the interior of the ocean). The prognostic partitioning framework adopted for this study allows us to track explicitly the source of dissolved inorganic carbon (DIC) and avoid including errors from assumptions made when using back-calculation techniques (e.g., Brewer 1978; Chen and Millero 1979; Gruber et al. 1996; Follows and Williams 2004; Duteil et al. 2012; Lauderdale et al. 2013). For example, the use of apparent oxygen utilization (AOU) to estimate the contribution of organic matter remineralization to total DIC relies on the assumption that surface O_2 is everywhere at equilibrium with the atmosphere. Ito et al. (2004a) showed that this assumption can lead to significant errors,

especially in high vertical mixing regions. Furthermore, the use of a prognostic preformed alkalinity tracer, in our study, eliminates the necessity to estimate such quantity through empirical relationships with other tracers as was done in the past (Gruber et al. 1996; Lauderdale et al. 2013).

Previous studies with coupled models compared simulations performed with either a fully biotic or with an abiotic ocean (Sarmiento and Le Quéré 1996; Sarmiento et al. 1998). Other studies separated the effects on the carbon cycle forced by different physical drivers using archived fields from a coupled model to force a carbon model (Matear and Hirst 1999) or ocean-only models forced with reanalysis atmospheric products (Lovenduski et al. 2008; Matear and Lenton 2008; Le Quéré et al. 2010). Our study expands the ideas behind these previous approaches by using detailed, explicit diagnostics of the mechanisms controlling ocean natural carbon storage and by using a coupled model that allows for realistic two-way physical feedbacks between the ocean and atmosphere systems. Our goal is to perturb only one aspect of climate at the time while leaving everything else untouched and free to evolve according to its full coupled response. Such an approach would not be possible with an ocean-only model where the rigidness of the atmospheric forcing imposed would result in a different outcome for sensitive processes such as, for example, open sea convection in the Southern Ocean (Hirabara et al. 2012).

In the next section, we give a theoretical explanation of the prognostic tracers that are used to disentangle the mechanisms governing ocean carbon storage. In section 3, we introduce the simulation design. Section 4 summarizes the changes to the global meridional overturning cells, which prove to be critical to the ocean carbon cycle. We then dissect the response of the components of DIC to physical perturbations, separating them into buoyancy-driven changes (section 5a), wind-driven changes (5b), solubility-driven changes (5c), and the total impact of climate change (5d). Here, we also explore the nonlinearities that prevent the sum of the perturbation simulations from being precisely equal to the total from the climate change simulation (5e) and discuss the differences between our method and back-calculation techniques (5f). Finally, we conclude in section 6 by contextualizing our results among earlier modeling studies and recent observational syntheses, exploring caveats on our results, and presenting our outlook for the future.

2. Theoretical background on oceanic carbon storage

The total DIC concentration of a parcel in the deep ocean results from the mixing of water masses formed at the surface ocean and the production and remineralization of organic matter along the water mass transport pathways (Iudicone et al. 2011). The biological pump transports carbon from the surface to the deep ocean via two mechanisms. The most important of these, called the soft-tissue pump, is driven by the planktonic production of organic matter at the ocean surface and its subsequent sinking and remineralization at depth. Quantitatively less important, the carbonate pump is maintained instead by the formation of planktonic calcium carbonate shells at the ocean surface and their dissolution at depth. Meanwhile, the solubility of CO_2 at the surface has an inverse relationship with both sea surface temperature (SST) and salinity (SSS). As a result, cold high-latitude surface waters hold more CO_2 than their warm, low-latitude counterparts. Thus, the sinking and/or subduction of water masses enriched in CO_2 beneath overlying warm waters help to maintain a vertical DIC gradient.

To better understand the processes at work, we apply a carbon partitioning framework based on the ideas of previous studies (Brewer 1978; Gruber et al. 1996; Ito and Follows 2005; Williams and Follows 2011; Lauderdale et al. 2013). The novelty of our approach is in the use of a set of prognostic tracers that allows an improved separation of carbon reservoirs by avoiding the errors implied in the offline calculations. We start by defining the preformed fraction of a tracer as the portion of the total that is transported into the ocean interior from the euphotic layer without having fueled primary productivity (Ito and Follows 2005; Marinov et al. 2006; Sarmiento and Gruber 2006; Goodwin et al. 2007; Marinov et al. 2008b; Kwon et al. 2011). Preformed tracers are set equal to the total tracer concentration at the ocean's surface and are conservative tracers in the ocean's interior. The remineralized fraction is given by the remineralization of the organic and mineral matter synthesized by primary productivity. Thus, the total dissolved inorganic carbon (DIC_{tot}) is defined as

$$DIC_{tot} = DIC_{pre} + DIC_{rem}, \tag{1}$$

where DIC_{rem} is formed by both the remineralization of carbon in the organic soft tissue synthesized by all phytoplankton types (DIC_{soft}) and the dissolution of the calcium carbonate shells of calcifying phytoplankton (DIC_{carb}):

$$DIC_{rem} = DIC_{soft} + DIC_{carb}. \tag{2}$$

The soft tissue contribution is related to remineralized phosphate (PO_4^{rem}) via a carbon:phosphorous stoichiometric ratio $r_{C:P} = 106$ (Anderson and Sarmiento 1994) according to

$$DIC_{soft} = r_{C:P} PO_4^{rem} = r_{C:P}(PO_4^{tot} - PO_4^{pre}). \tag{3}$$

The carbonate contribution is obtained from alkalinity (Alk) and PO_4 following

$$\begin{aligned} DIC_{carb} &= 0.5(Alk_{rem} + r_{N:P}PO_4^{rem}) \\ &= 0.5[Alk_{tot} - Alk_{pre} + r_{N:P}(PO_4^{tot} - PO_4^{pre})], \end{aligned} \tag{4}$$

where the term $r_{N:P}(PO_4^{tot} - PO_4^{pre})$ accounts for the impact of the soft-tissue pump on alkalinity and $r_{N:P}$ is the nitrogen:phosphorous stoichiometric ratio (here assumed as $r_{N:P} = 16$). Since the remineralization of organic matter (production of NO_3^-) decreases Alk, the sign of this correction is positive (Sarmiento and Gruber 2006). This conceptual framework includes one additional source of complexity: the residence time of a water parcel at the sea surface is of the same order as the time scale for the equilibration of CO_2 between atmosphere and the sea surface (Ito et al. 2004b). The similarity of these time scales can create a negative or positive DIC disequilibrium (DICdis; i.e., undersaturation or supersaturation), depending on the Lagrangian history of a water parcel. Undersaturation occurs when a water parcel moving toward high latitudes at the surface cools and sinks or subducts into the ocean interior before equilibrating with the atmosphere (Follows and Williams 2004). This negative disequilibrium is reinforced by biological consumption of CO_2, which is transferred via sinking particles to water masses in the subsurface and converted to DIC_{rem}. On the other hand, supersaturation occurs when deep waters upwelled or mixed vertically to the surface arrive with high concentrations of DIC_{rem}, thereby creating a positive DIC_{dis} relative to the saturation state of the surface waters (DIC_{sat}). If the equilibration time scale of the air–sea gas exchange is longer than the residence time of the water masses at the ocean's surface, then the water masses reenter the ocean interior supersaturated in DIC. Hence, a positive disequilibrium in DIC is built up by biologically stored carbon even if, after touching surface, it has been relabeled as DIC_{pre}. We define DIC_{dis} as

$$DIC_{dis} = DIC_{pre} - DIC_{sat}, \tag{5}$$

where DIC_{sat} is the concentration of DIC at the surface of the ocean when equilibrium with the pCO_2 of the overlying atmosphere is assumed. Note that DIC_{sat} is also solved prognostically in our model to avoid including nonlinearities arising from mixing processes.

3. Model and experimental design

a. Coupled climate model

All simulations were carried out using CM2Mc (Galbraith et al. 2011) a nominal three-degree coupled atmosphere–ocean–carbon cycle model. CM2Mc is the Geophysical Fluid Dynamics Laboratory Climate Model version 2 (GFDL CM2) with Modular Ocean Model version 4p1 (MOM4p1) at coarse resolution. CM2Mc uses the same physical oceanic and atmospheric code as the Earth System Model with the Modular Ocean Model (ESM2M; Dunne et al. 2012), with minor alterations as required to adjust to the coarser discretization. The CM2Mc ocean uses a tripolar grid with enhanced latitudinal resolution near the equator and at midlatitudes, benefiting the resolution of equatorial currents. There are 28 vertical levels unevenly distributed with a finer resolution toward the surface. Eddy mixing is represented using the parameterization of Gent and McWilliams (1990) with a spatially varying diffusion coefficient (Griffies et al. 2005). The atmosphere employs the M30 grid, with a latitudinal (longitudinal) resolution of 3 (3.75) degrees and 24 vertical levels. The CM2Mc land component is the Land Dynamics model of Milly and Shmakin (2002), which includes a river routing scheme but no terrestrial ecosystem. Ocean biogeochemistry is solved by the Biogeochemistry with Light, Iron, Nutrients and Gases (BLING) model (Galbraith et al. 2010), an intermediate complexity biogeochemistry model constructed around a core of only four prognostic tracers and including macronutrient limitation, iron limitation, light limitation, and photoadaptation. BLING is fully prognostic and can be used with an additional module to simulate carbon chemistry and preformed tracers for PO_4, DIC, and Alk, which allows the separation of the contribution of the individual carbon pumps to the total DIC, as shown in section 2. Details on the formulation of the carbon cycle are given in appendix A.

b. Experimental design

We seek a mechanistic understanding of the relative roles of surface warming, wind, and buoyancy forcing, through their effect on global circulation and CO_2 solubility at the ocean surface, in the functioning of the natural carbon pumps over the twenty-first century. To this end, we run the following simulations for the period 1860–2100:

(A) *Control* A full control simulation in which all forcing variables are kept constant at preindustrial (1860) levels.

(B) *Climate* A climate change simulation using the forcing data recommended by phase 5 of the Coupled Model Intercomparison Project (CMIP5). We used atmospheric prescribed concentrations for greenhouse gases following the Historical forcing (1860–2005) plus the representative concentration pathway 8.5 (RCP8.5, 2006–2100) which is based on the A2R emission scenario detailed in Riahi et al. (2007). Ozone was also prescribed from historical data and

future projections, including contemporary depletion and future gradual recovery (Cionni et al. 2011).

(C) *Wind* A positive wind perturbation experiment in which forcing is prescribed as in Control, but a time-varying wind stress perturbation is applied to the ocean.

(D) *Buoyancy* Forcing is prescribed as in Climate, but the wind change is suppressed. This suppression is achieved by adding a time-varying wind stress perturbation to the ocean, of the same magnitude but opposite sign as the anomaly in Wind. Thus, the forcing for this simulation can be thought of as Climate − Wind.

(E) *Gas_exchange* A solubility perturbation experiment where forcing variables are prescribed as in Control, but a time-varying sea surface temperature and salinity perturbation is imposed to the CO_2 gas exchange calculations.

Growing greenhouse gases over the twenty-first-century impact the physical climate in simulations B, C, and D, and CO_2 solubility in simulation E. However, in all simulations the model's air–sea gas exchange formulation uses preindustrial CO_2 concentrations of 286 ppmv (i.e., the simulations explicitly exclude the penetration of anthropogenic carbon in the ocean). Thus, the present paper deals exclusively with the response of natural carbon storage to climate change; the anthropogenic carbon penetration in the ocean and its response to future climate will be discussed separately in a follow-up paper.

We run three ensemble members for each experiment. Each member is started from initial conditions taken at different points of a 1000-yr preindustrial simulation segment performed after the end of the spinup period (3500 yr). To compute the time-varying perturbations used in experiments C through E we start by running the Control and Climate simulations. We next compute the anomalies in vector wind stress, SST, and SSS as the differences in monthly means between the Climate and Control simulations. To remove the interannual signal caused by the main climate modes of variability, we smooth these anomalies by calculating 20-yr running means, for each month, over the period 1860–2100 (Fig. 1). The smoothed anomalies are then applied at each ocean time step after time interpolation. The wind stress anomalies are applied when the momentum fluxes are passed from the atmosphere to the ocean and do not directly interfere with any other oceanic process. The atmosphere does not feel the wind perturbation except for any feedback resulting from changes in ocean circulation, as in Delworth and Zeng (2008). The SST and SSS perturbations are applied to the respective prognostic fields computed by the ocean model when these are passed to the CO_2 gas exchange routine in the Gas_exchange experiment.

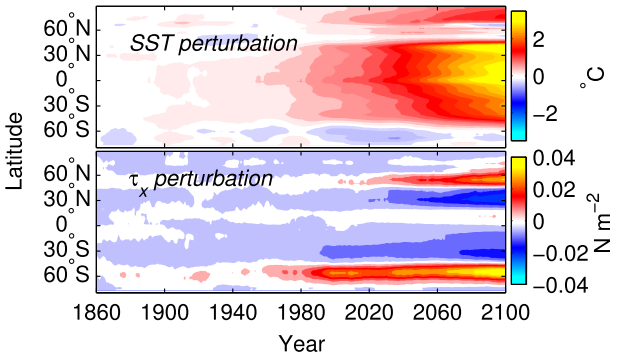

FIG. 1. Time evolution of the perturbations used in the (top) Gas_exchange and (bottom) Wind simulations. Here, only SST and the zonal component of the wind stress, τ_x, are shown.

As described in the introduction, prescribed historical ozone depletion in the troposphere drives the poleward shift and strengthening of the Southern Hemisphere Westerlies at the end of the twentieth century (Thompson and Solomon 2002). During the twenty-first century, ozone concentrations are prescribed to gradually recover while greenhouse gas concentrations are still increasing (Cionni et al. 2011). This results in competing effects on the Southern Hemisphere atmospheric circulation, with uncertain trends (Son et al. 2009; Karpechko et al. 2010; Arblaster et al. 2011; Polvani et al. 2011). In our model, the end of the twenty-first century sees stronger and poleward westerlies in both hemispheres (Fig. 1). The SST perturbation shows the largest warming over the tropics and subtropics. Weaker surface warming south of 50°S and north of 50°N can be partially explained by the enhanced mixing of deeper cold water caused by the poleward shift and increase of the westerlies and partially by the decrease in North Atlantic Deep Water (NADW) formation, which slows the poleward transport of warm waters (Palter et al. 2014).

Two of the perturbation experiments affect the ocean circulation by altering the wind stress over the ocean. In one case the perturbation is applied with a positive sign on a preindustrial circulation (Wind) while in the other case the same perturbation is applied with a negative sign on a climate change circulation (Buoyancy). The goal of the simulations is to separate the effects on circulation caused by changes in wind patterns from those caused by changes in heat and freshwater fluxes. In the Buoyancy experiment we choose not to perturb directly heat and freshwater fluxes but rather to let these evolve coherently with the changing climate of the coupled model. Instead, we perturb the wind stress applied to the ocean in such a way as to keep it at preindustrial level. We note that both the wind and buoyancy effects could have been estimated by altering heat and freshwater fluxes instead of the wind stress. However, the ocean–atmosphere coupling is tighter for heat fluxes than for

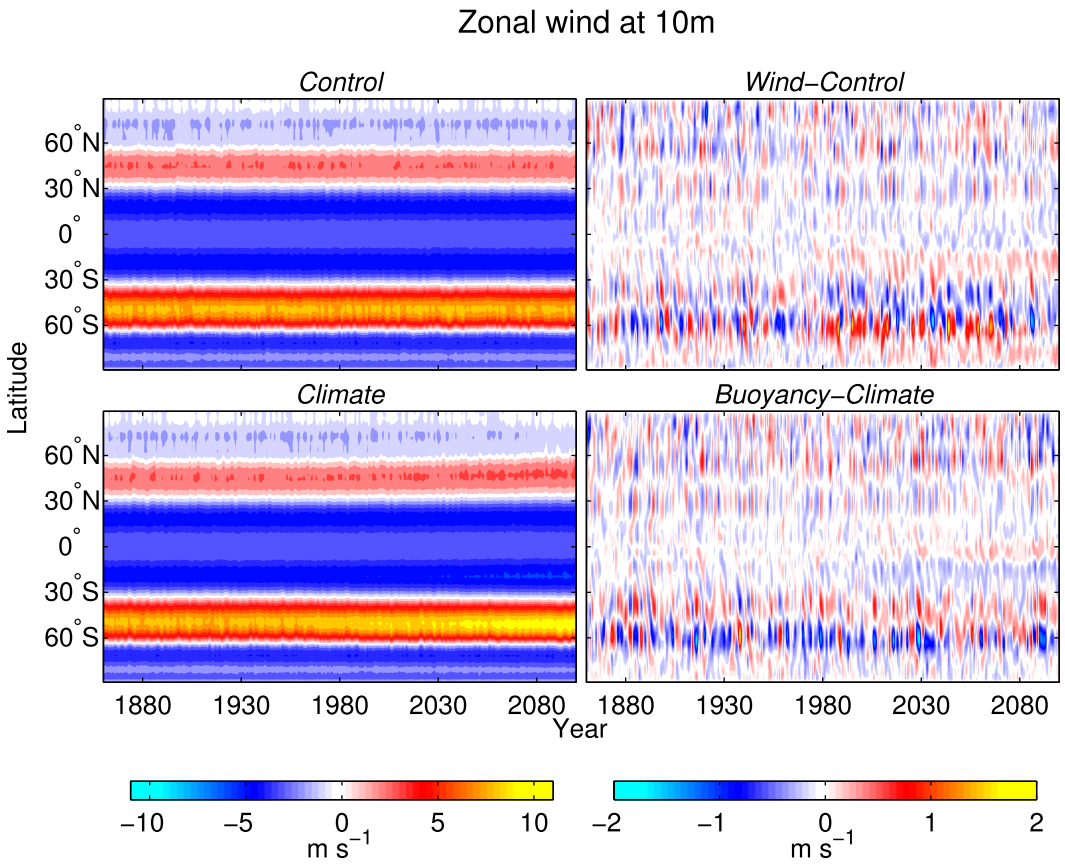

FIG. 2. Wind feedback from the ocean to the atmosphere for a positive wind stress perturbation (Wind) and for a negative wind stress perturbation (Buoyancy). The zonal wind predicted by the atmospheric model is not affected by the wind stress perturbation imposed except for any feedback resulting by the changes in ocean circulation. This feedback is quantified here by comparing the 10-m zonal wind speeds in the (upper right) Wind simulation to the Control simulation and (lower right) Buoyancy simulation to the Climate simulation. These differences are generally less than 10% of the wind speed in either run and show no trend.

momentum fluxes. If we performed a perturbation of the heat flux, the feedback from the ocean to the atmosphere would affect the heat flux itself, leading to a difficult interpretation of the oceanic response. On the other hand, the feedback from the perturbation of the momentum flux arises only through its influence on ocean mixing and circulation, which results in a change in SST and SSS. This, in turn, affects the heat and freshwater fluxes, which modifies the winds and, eventually, feedback onto the ocean surface. We quantify this feedback by comparing the zonal wind (rather than the perturbed wind stress) predicted by the atmospheric model between (a) the Wind and Control simulations in the case of the positive wind perturbation and (b) the Buoyancy and Climate simulations in the case of the negative wind perturbation (Fig. 2). There is no clear trend in time in the zonal wind difference in either case (a) or (b), despite the time-varying perturbations applied to the wind stress in both cases. Therefore, the feedback from the ocean to the atmosphere, caused by the wind stress perturbations applied to the ocean, has a small effect not discernible from the internal variability of the model.

These considerations also strengthen our motivation for performing these simulations with a fully coupled atmosphere–ocean model instead of using a less computationally expensive ocean-only configuration forced with atmospheric fields obtained from the coupled model. In fact, some of the major climate responses may not evolve in the latter configuration as they do in the former. An important example in our study is represented by the convective cycles of the Southern Ocean, which exert a strong control on Southern Ocean carbon. Convection is an inherently coupled process, whereby the atmosphere warms due to extraction of heat from the ocean and this warming can ultimately slow convection, processes difficult to properly simulate in an ocean-only model (Hirabara et al. 2012). The warm surface air temperature resulting from convection in the coupled model

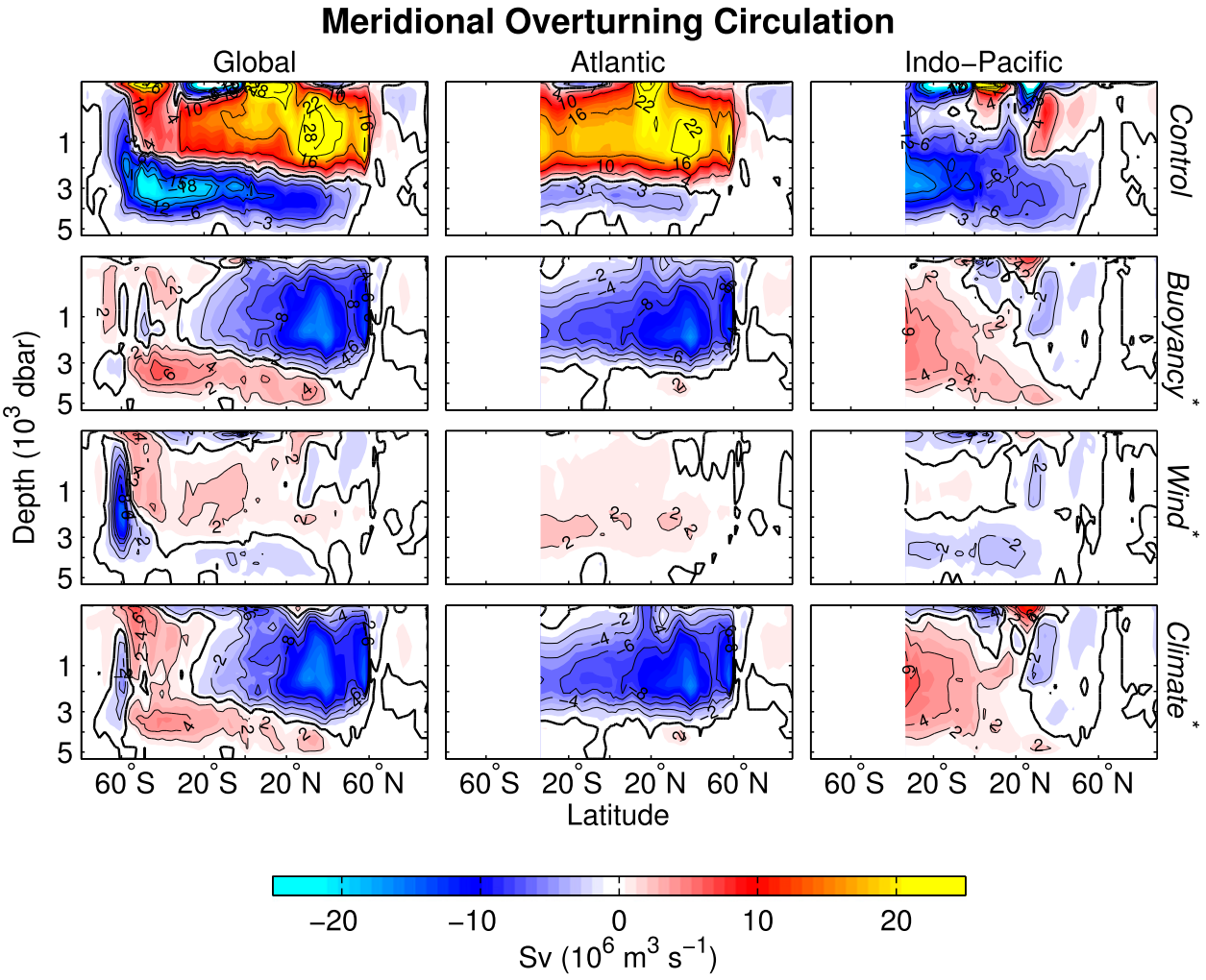

FIG. 3. Meridional overturning circulation for the (left) global ocean, (middle) Atlantic Ocean, and (right) Indo-Pacific Oceans, for the (top) preindustrial state, and for anomalies with respect to the preindustrial state for the (second row) Buoyancy, (third row) Wind, and (bottom) Climate experiments. For each panel we show the ensemble mean averaged over the period 2081–2100. Note that the upper 1000 dbar are amplified on the vertical axis.

would suppress convection (via reduced air–sea temperature gradient) if that temperature field were applied as a forcing field in an ocean-only model.

Finally, in the Gas_exchange experiment we deliberately choose not to perturb alkalinity, which might have a significant impact on CO_2 solubility, because we want each experiment to represent a purely physical perturbation of the climate to the ocean carbon cycle. Alkalinity is affected also by biogeochemical processes so, strictly speaking, a change in alkalinity is not a purely physical perturbation on the gas exchange but rather an indirect effect comparable to a feedback.

Climate-driven changes in the natural DIC storage can be attributed to different processes by combining results from the five experiments. From here on, when the experiment name appears with an asterisk (e.g., Climate*) it indicates that the result from the Control experiment was subtracted and the quantity shown is an anomaly relative to the unforced experiment. One exception is that Buoyancy* refers to the difference: Buoyancy* = Buoyancy − Gas_exchange. This definition allows the isolation of changes in the various DIC reservoirs caused only by buoyancy-driven changes in circulation because the effects of changes in CO_2 solubility are taken into account in Gas_exchange.

4. Response of the global meridional overturning circulation

The response of the global meridional overturning circulation (MOC) to wind, buoyancy, and total climate change over the twenty-first century is shown in Fig. 3.

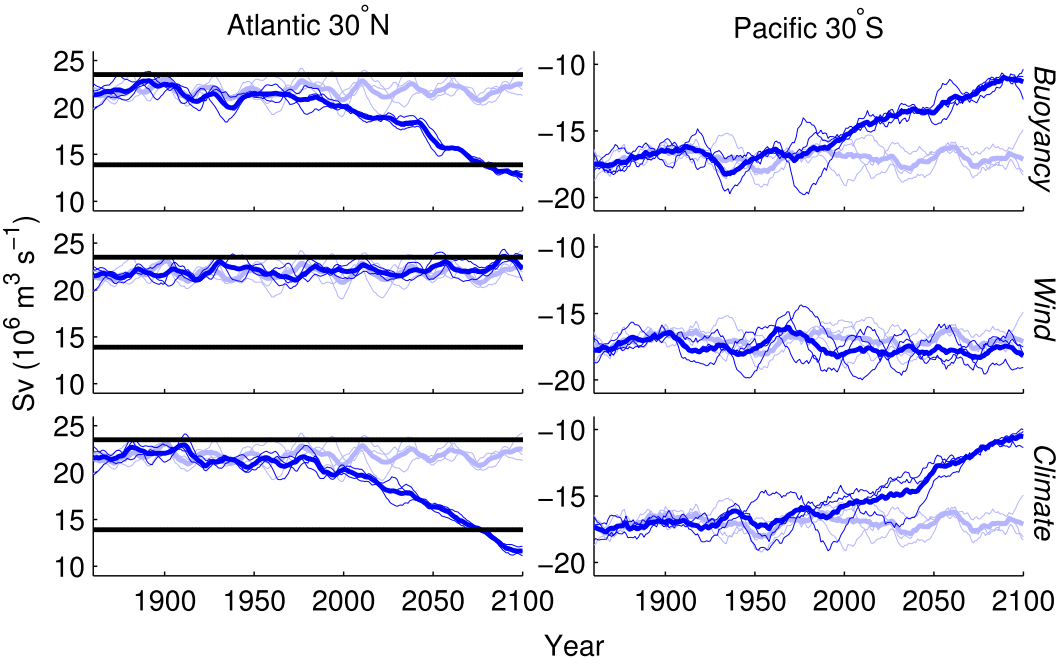

FIG. 4. Meridional overturning circulation index as the maximum annual mean taken at 30°N in the Atlantic Ocean for the upper cell and at 30°S in the Pacific Ocean for the lower cell. Dark blue refers to the Buoyancy, Wind, and Climate simulations and light blue to the Control simulation. Thick lines refer to the ensemble mean while thin lines refer to single ensemble members. Each time series is filtered by an 11-yr running mean. Horizontal black lines in the left panel refer to the temporal variability range for the RAPID data at 26.5°N for the period 2004–08 (18.7 ± 4.8 Sv; Rayner et al. 2011).

The buoyancy-driven changes dominate the overall effect of twenty-first century climate change on circulation (cf. Buoyancy* and Climate* in Fig. 3), with a localized, yet discernible, wind-driven acceleration of the shallow circulation of the Southern Ocean (Wind*). Changes in circulation driven by heat and freshwater fluxes (Buoyancy*) cause a slowing of the upper and lower overturning cells, with most of the signal in the upper cell associated with a marked decrease in the NADW formation rate, and changes in the lower cell primarily driven by the Indo-Pacific sector. By 2100 the Atlantic MOC strength (defined as the annual mean maximum volume transport streamfunction at 30°N) weakens by ~40% in Climate compared to the mean of the historical period (1860–2005), due almost entirely to changes in buoyancy forcing (Fig. 4). An observational estimate of the variability range of the MOC strength derived from the Rapid Climate Change Programme (RAPID) array data (Rayner et al. 2011) is also shown in Fig. 4 for comparison. Under the same scenario (RCP8.5), CMIP5 models show a range of relative weakening of the Atlantic MOC from 15% to 60% (Cheng et al. 2013). The corresponding weakening of the lower cell of the MOC in our model (defined here as the annual mean northward maximum volume transport streamfunction at 30°S in the Pacific Ocean) is ~36% (Fig. 4).

Fighting the buoyancy-forced slowdown in meridional overturning, an increase and poleward shift in the Southern Hemisphere westerlies (Wind*) causes an acceleration of both the upper and the lower cells of the MOC through changes in Ekman transport, particularly north of the Polar Front (PF). In isolation, this wind-driven acceleration enhances the upwelling of CDW as well as the downward transport along the Antarctic Bottom Water (AABW) formation pathway, in qualitative agreement with previous results from similar experiments (Delworth and Zeng 2008; Farneti et al. 2010). However, these wind-driven changes are generally much smaller than the buoyancy-driven changes of the opposite sign (Figs. 3 and 4).

The transport associated with the Antarctic Circumpolar Current (ACC), calculated as the zonal transport across the entire Drake passage integrated at all depths, is 160 ± 6 (Sv; 1 Sv ≡ 10^6 m^3 s^{-1}) for the Control simulations. In the case of the Wind simulations this goes to 178 ± 7 (Sv), increasing by about 11%. For the Buoyancy simulations the ACC transport it is 142 ± 1 (Sv), representing a decrease of about 11%. For the Climate simulations it is 160 ± 3 (Sv), which does not differ significantly from the preindustrial ACC transport. This suggests that in our simulations the wind-driven ACC acceleration is counterbalanced by a buoyancy-driven slowdown. In an extensive analysis of CMIP5 models,

TABLE 1. Global ocean content of each DIC component in the Control simulation (first line) and absolute changes for each simulation. Columns 4 and 5 show the corresponding estimates made using back-calculation techniques. Units are Pg C and ± one standard deviation relative to the three ensemble members is reported.

DIC_{tot}	DIC_{pre}	DIC_{rem}	DIC_{rem}^{back}	DIC_{pre}^{back}	
36 859 ± 4	35 134 ± 5	1734 ± 9	2177 ± 7	34 882 ± 4	Control
+20 ± 3	−80 ± 3	+100 ± 1	+76 ± 3	−56 ± 5	Buoyancy*
−3 ± 3	−3 ± 6	−0 ± 8	+1 ± 5	−4 ± 2	Wind*
−35 ± 2	−35 ± 2	+0 ± 0	+0 ± 0	−36 ± 2	Gas_exchange*
−20 ± 3	−116 ± 3	+96 ± 6	+73 ± 6	−93 ± 3	Climate*

Downes and Hogg (2013) showed that a weakened ACC is a common response to increasing freshwater and heat fluxes in many CMIP5 models, while the ACC response to winds is less certain. Their analysis separated these effects statistically (i.e., via linear regression) rather than via manipulation of the model forcing, as was done here.

5. Response of the natural carbon storage

In this section we describe and discuss changes in the distribution and total ocean content of DIC components in response to simulated climate-driven perturbations. We point out once more that, in order to isolate the response of the ocean natural carbon cycle, we have deliberately ignored the uptake of anthropogenic CO_2. When such uptake is computed in a parallel set of simulations (not analyzed here), the Climate experiment shows an accumulated total ocean carbon uptake of 516 Pg C over the period 1860–2100 while the Control experiment gives 582 Pg C over the same period. The difference (66 Pg C) between these two estimates is partly (20 Pg C) due to climate-driven changes in the ocean natural carbon cycle and is the focus of this study. Table 1 shows a summary of results.

a. Response to buoyancy-driven changes

The redistribution of DIC components in the Climate simulations is caused primarily by the buoyancy-driven changes in circulation while wind-driven changes have an opposite but small effect. The overall response to the change in buoyancy forcing (Figs. 5 and 6, first row, Buoyancy*) is an accumulation of DIC_{rem} (+100 Pg C), partially compensated by a decrease of DIC_{pre} (−80 Pg C). An important consequence of altered buoyancy forcing is the reduction of convective mixing at high latitudes in the Southern Ocean, North Atlantic, and North Pacific. Here, under preindustrial conditions, winter convective mixing allows for DIC_{rem} accumulated at depth to outgas to the atmosphere while also bringing nutrients to the euphotic zone and increasing biological productivity and DIC remineralization. Therefore, convective mixing is linked to both a sink and a source for the oceanic reservoir of DIC_{rem}. A reduction in high-latitude convective mixing causes a slowdown in the rate of production of DIC_{rem}, due to a decrease in nutrients and associated export production. But such a slowdown also decreases the amount of DIC_{rem} that is brought to the surface and partially lost to the atmosphere through gas exchange after being converted into DIC_{pre}.

We quantify these two effects at the end of the twenty-first century to understand the increase in DIC_{rem} due to buoyancy-driven changes in circulation (Buoyancy*), for different latitudinal bands (Fig. 7). The red lines represent the time integrated decrease in export production, that is, the total decrease in the biological source of DIC_{rem} throughout the period simulated. Blue lines represent the change in the distribution of DIC_{rem} at the end of the twenty-first century. The changes are the result of the decrease in export production (DIC_{rem} source) and the decrease in DIC_{rem} outgassing (sink). As can be deduced by subtracting the red line from the blue line, the decrease in the sink of DIC_{rem} has a dominant effect over the decrease in the source of DIC_{rem}, in agreement with the coupled model study of Matear and Hirst (1999). Only in the upper 100 m (not shown in Fig. 7) everywhere and in the upper 900 m at low latitudes (40°S–40°N) is the net result a decrease in DIC_{rem}, which, summed with the decrease in DIC_{pre}, results in a decrease of DIC_{tot}. The buoyancy-driven decrease in DIC_{pre} is associated with both reduced vertical mixing and lower rates of deep and intermediate water formation, resulting in a general decrease of the transport of DIC_{pre} from the surface to the interior of the ocean. As already stressed by Marinov et al. (2006, 2008a) and confirmed here, export production is not a good indicator of the ability of the biological pump to store carbon in the ocean: in these simulations the storage of remineralized DIC increases while export production declines under future climate change.

b. Response to wind-driven changes

One of the most striking changes triggered by the wind perturbation alone is a shift in the region of deep convection in the Southern Ocean from the Weddell Sea

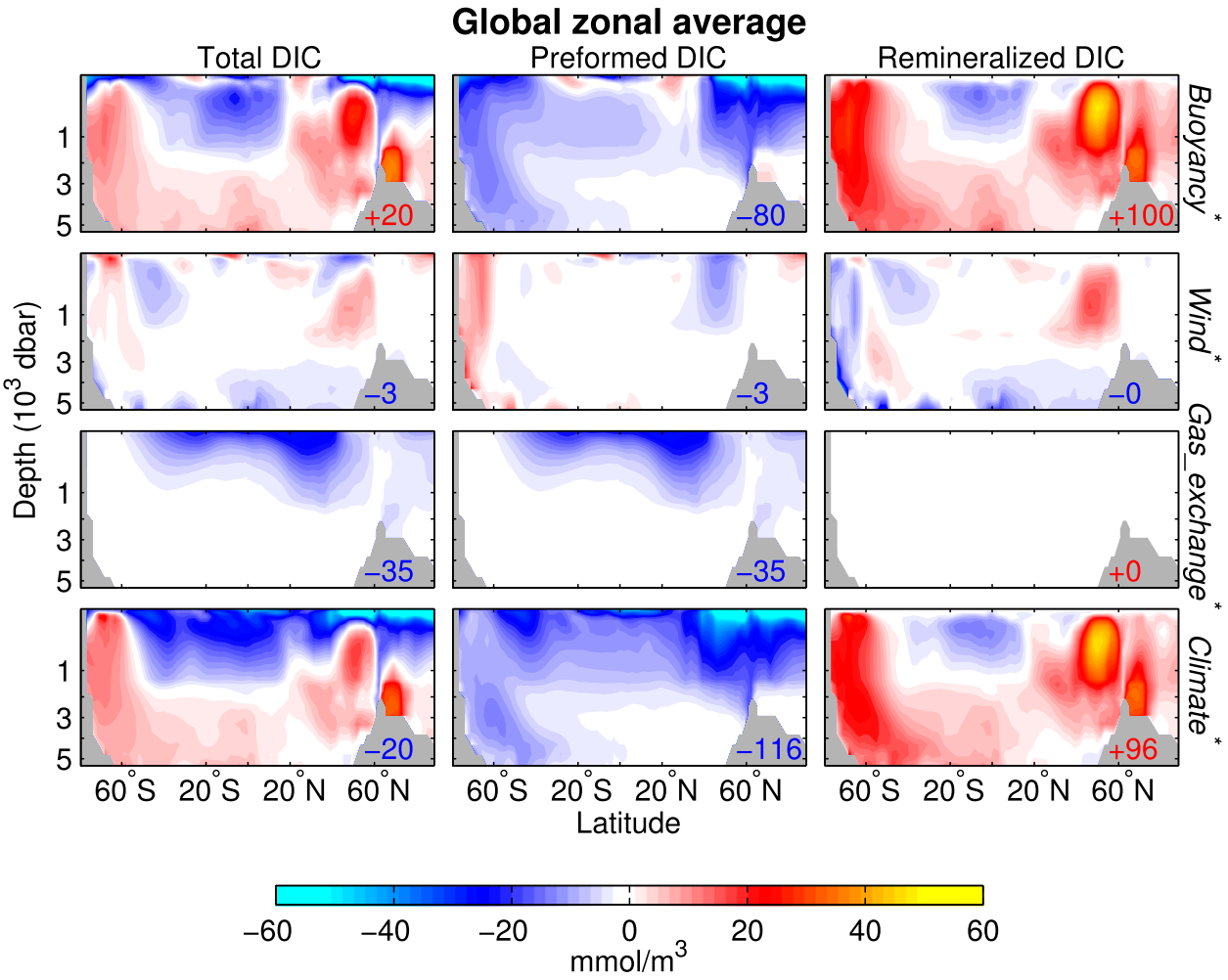

FIG. 5. Zonal average of DIC components anomalies with respect to the preindustrial state. Numbers refer to total DIC gained or lost (Pg C). The figure shows the ensemble mean averaged over the period 2081–2100.

(Atlantic sector) to the Ross Sea (Indo-Pacific sector). In contrast, in the Buoyancy simulation, open ocean convection in the Southern Ocean stops entirely, a common trend in CMIP5 models subjected to RCP8.5 forcing, as we have discussed separately (de Lavergne et al. 2014).

Because the wind perturbation enhances vertical exchange in the Indo-Pacific sector of the Southern Ocean the responses of the DIC pools are opposite in the Wind and Buoyancy simulations (Fig. 6). In the Southern Ocean, CDW that reaches the surface at the polar front has pCO_2 higher than that of the atmosphere because it has accumulated DIC_{rem} along its interior circulation pathways for hundreds to thousands of years. However, the long equilibration time scale of air–sea CO_2 gas exchange (between 6 months and 1 year) does not allow all of the excess DIC to escape before the water sinks again along the AABW formation pathway. Once at the surface, a portion of the CDW's DIC_{rem} load is outgassed to the atmosphere and the remainder is relabeled as DIC_{pre}. Separating DIC_{pre} into its DIC_{sat} and DIC_{dis} components [see Eq. (5)] reveals a positive disequilibrium that is injected again into the interior of the ocean along the AABW formation pathway. Strengthened Southern Hemisphere westerlies accelerate both the upwelling at the PF and deep convection in the Ross Sea, increasing the positive disequilibrium along the AABW formation and export pathway (Fig. 8, right column). Part of the positive anomaly in DIC_{pre} is also due to the increase in DIC_{sat} as a result of a decrease in temperature caused by the enhanced vertical mixing.

The evolution of an ideal age tracer supports this explanation (Fig. 9). The ideal age tracer is set to zero in the ocean model's mixed layer and ages at a rate of one year per year in the ocean's interior; otherwise, it is transported and mixed as any other passive tracer. In response to the wind perturbation (Wind*), an

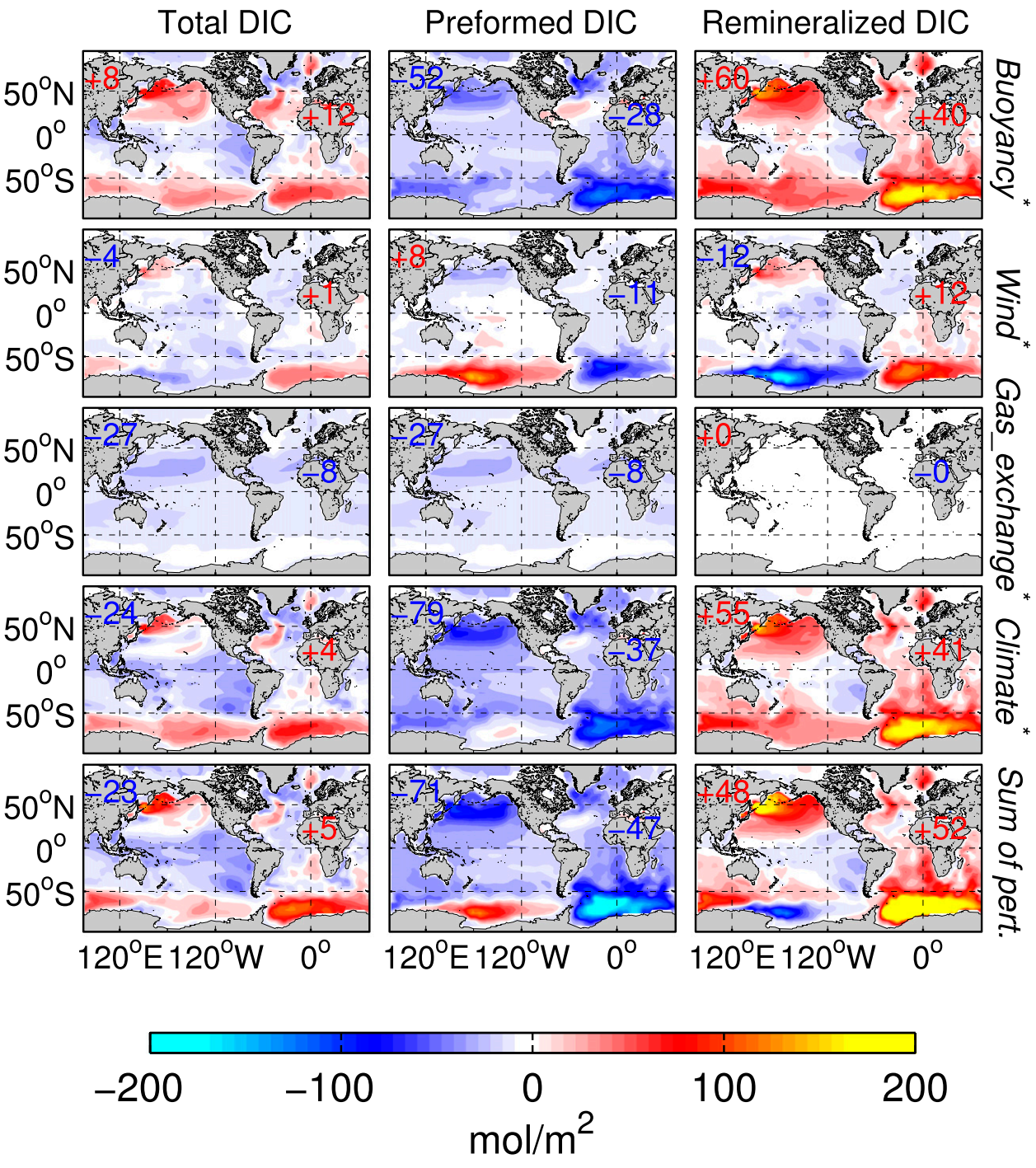

FIG. 6. Vertically integrated DIC components anomalies with respect to the preindustrial state for each experiment. The fifth row is the sum of all partial perturbations (the first three rows). Numbers refer to total DIC gained or lost (Pg C) for the Indo-Pacific (numbers over Asia) and the Atlantic (numbers over Africa). The figure shows the ensemble mean averaged over the period 2081–2100.

acceleration of the lower cell of the MOC allows for younger water to fill the Indo-Pacific sector of the Southern Ocean. These physical changes lead to an enhanced penetration of DIC_{pre} into the interior, and a decrease in the amount of DIC_{rem} that a water parcel can accumulate. The Wind* decrease in DIC_{rem} is stronger than the compensating increase in DIC_{pre} with a net decrease of DIC_{tot} as a result. This is in qualitative agreement with previous modeling studies that found a decrease in the Southern Ocean CO_2 sink over the last two decades of the twentieth

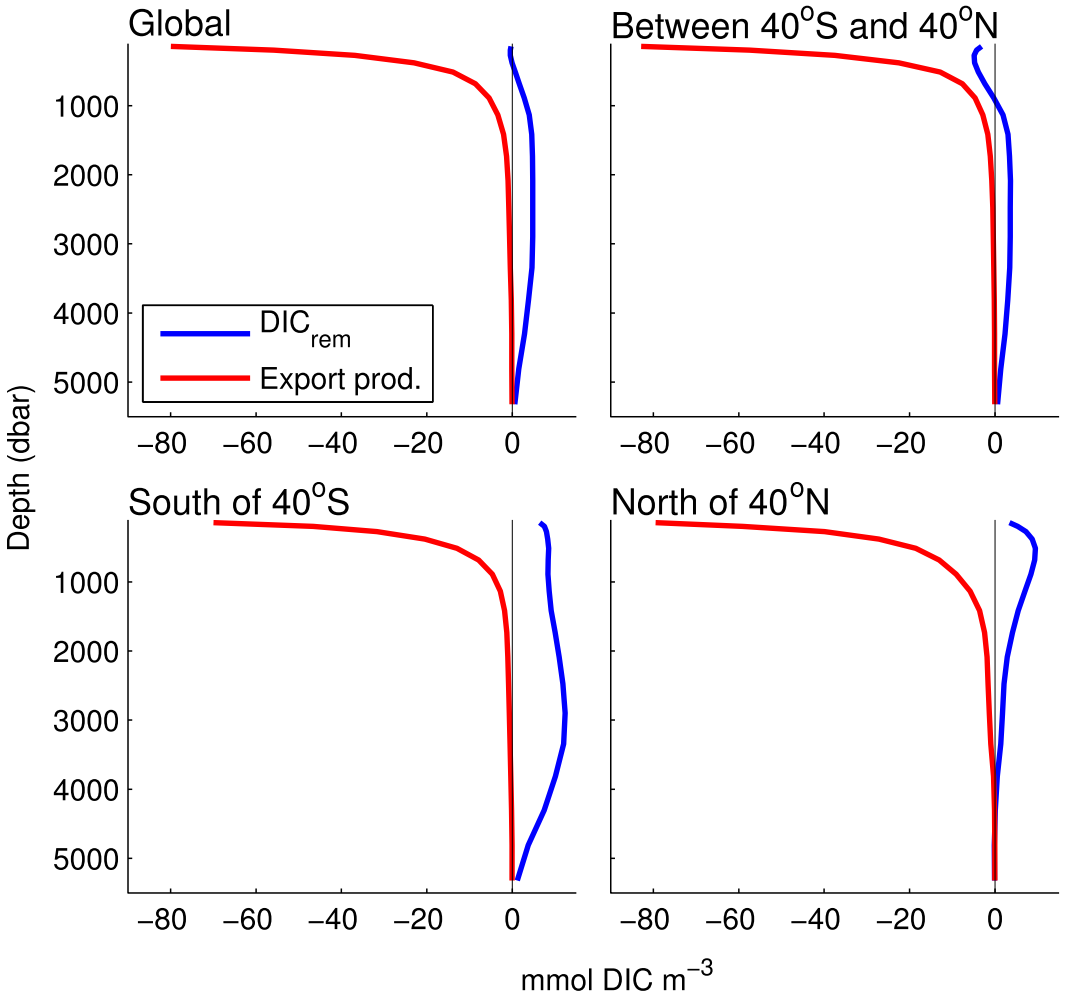

FIG. 7. Time integrated (1860–2100) decrease in export production (red lines) and change in the distribution of DIC_{rem} at the end of the twenty-first century (2081–2100 average; blue lines) for the Buoyancy simulations.

century, in response to the observed increase and shift poleward of the southern westerlies (Wetzel et al. 2005; Lovenduski et al. 2008; Le Quéré et al. 2010).

However, the overall impact of the twenty-first-century wind stress perturbation on global carbon storage is weak because of a competition between differing responses in the Atlantic sector of the Southern Ocean, where the wind perturbation suppresses convection, and Indo-Pacific sector, where the wind stress perturbation initiates deep convective mixing (Figs. 6 and 8). The cessation of open ocean convection in the Weddell Sea is reflected by the increase in water age (Fig. 9, middle row). The increase in age allows for the accumulation of DIC_{rem} and a symmetric, but smaller decrease in DIC_{pre} in the Atlantic sector of the Southern Ocean. The decrease in DIC_{pre} is caused by a decrease in DIC_{dis} south of the PF, reflecting a reduced source of DIC_{rem} to the surface via CDW, more time to equilibrate with the atmosphere at the surface, and cessation of DIC_{dis} advection via AABW to the deep ocean. In agreement with the Weddell and Ross Sea asymmetry, an observational synthesis over the period 1980–2008 showed that in the Indo-Pacific sector of the Southern Ocean, a reduction in CO_2 uptake is associated with strengthened westerlies, while in the more stratified Atlantic sector, enhanced uptake is associated with increased biological production and reduced vertical supply (Lenton et al. 2012). The other region notably influenced by the wind stress perturbation is the north Pacific (Fig. 8), where the imposed wind stress anomaly also reduces vertical mixing, with analogous consequences to those in the Weddell Sea.

c. *Response to solubility-driven changes*

The final element of twenty-first-century climate change that we need to account for is the effect of SST and SSS

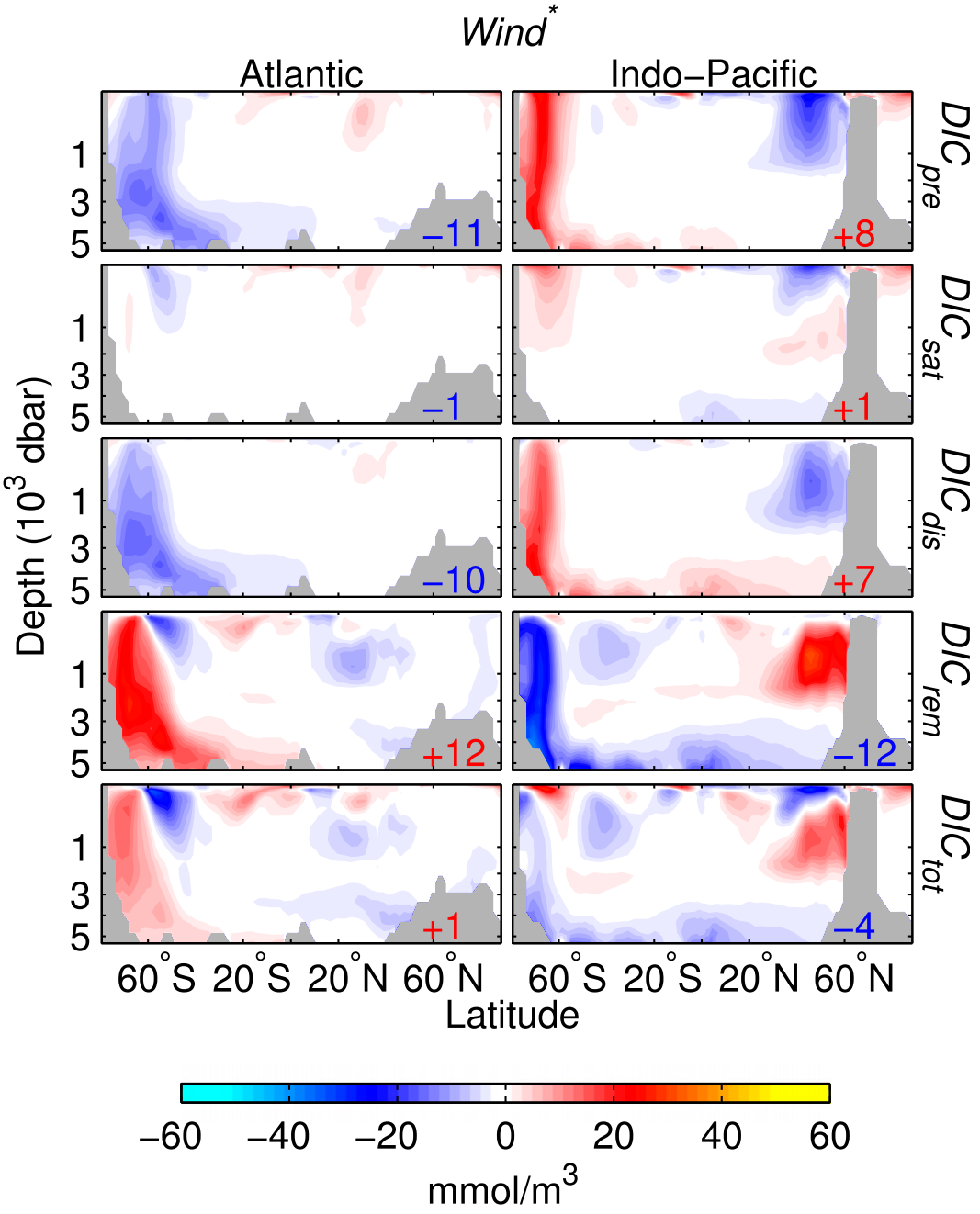

FIG. 8. Basin-specific zonal averages of DIC components anomalies with respect to the preindustrial state in the Wind experiment. Numbers refer to total mass gained or lost (Pg C) for each DIC component. Note that here the two components forming DIC_{pre} are also shown [see Eq. (5)]. The figure shows the ensemble mean averaged over the period 2081–2100.

changes on the chemical solubility of CO_2 at the ocean surface (experiment Gas_exchange). Increasing SST (and to a lesser degree SSS) particularly in the subtropics (Fig. 1) results in reduced solubility of CO_2 at the surface and a decrease of DIC_{pre} within the thermocline between 45°S and 45°N (Figs. 5 and 6). This decrease extends to a greater depth north of the equator, reflecting a stronger simulated upper ocean warming in the Northern Hemisphere (Fig. 1).

d. Response to full Climate change

Our experiments suggest that on the centennial time scale and in the global average, slower Antarctic and North Atlantic overturning leads to a more efficient

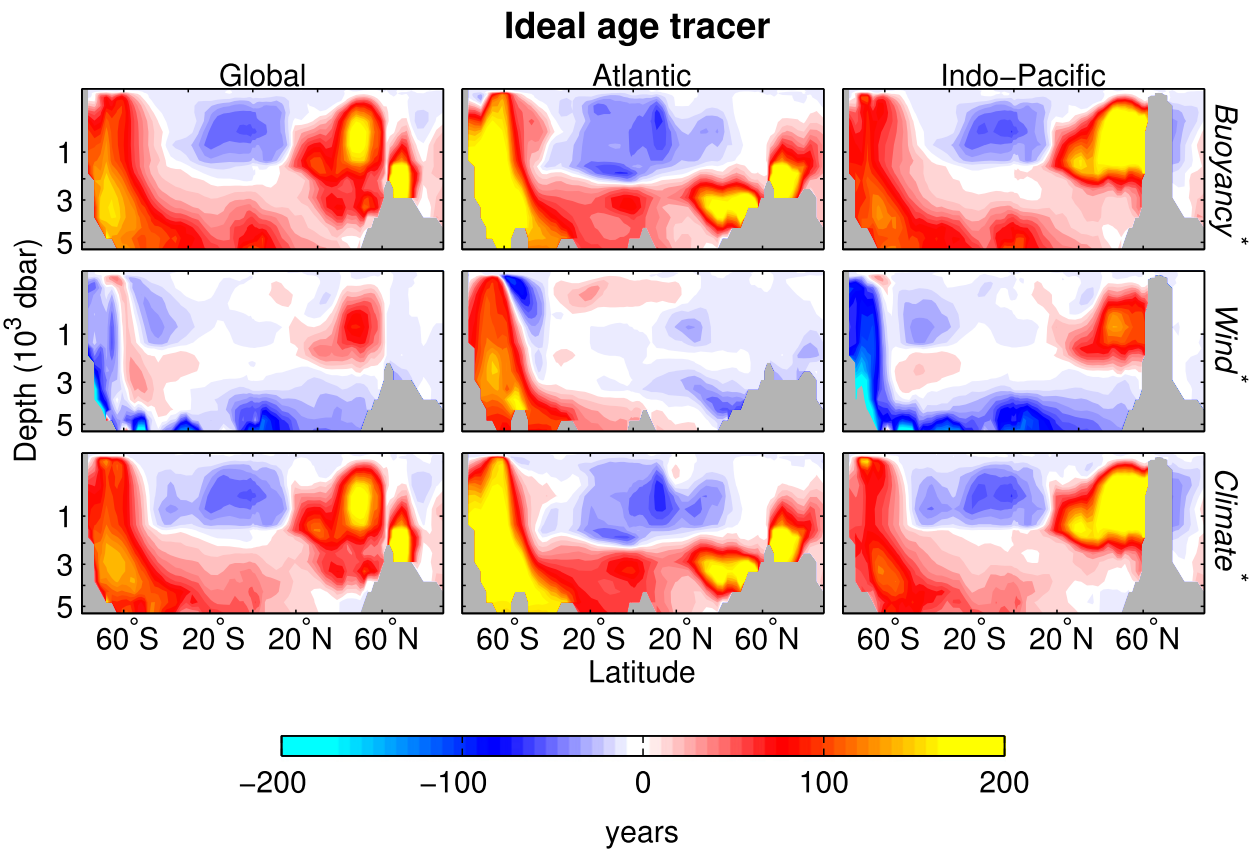

FIG. 9. Zonal averages for the changes with respect to the preindustrial state of the ideal age tracer in each experiment: (left) global, (middle) Atlantic Ocean, and (right) Indo-Pacific Ocean. The figure shows the ensemble mean averaged over the period 2081–2100.

biological pump (i.e., more DIC_{rem} storage), despite decreasing export production. This result can be thought of as broadly analogous to a decrease in the vertical mixing rate in the three-box model of Sarmiento and Toggweiler (1984), which strengthens biological carbon storage by essentially the same mechanism.

When considering changes in the natural carbon storage induced by changes in circulation only (i.e., Wind or Buoyancy simulations) the absolute response of DIC_{pre} is always weaker and of opposite sign to that of DIC_{rem} (see numbers in Figs. 5 and 6). This is because for a given perturbation in the circulation, regardless of the sign of the perturbation, the resultant DIC_{pre} anomaly is partially erased by gas exchange at the surface.

Indeed, reduced vertical mixing decreases the exchange of DIC_{rem} with the surface and its conversion to DIC_{pre} (thereby increasing DIC_{rem} and decreasing DIC_{pre} concentrations), but, at the same time, reduces the amount of DIC_{pre} outgassing to the atmosphere (thereby making the positive perturbation to DIC_{rem} larger than the negative perturbation to DIC_{pre}). Alternatively, we can consider again the separation of DIC_{pre} into DIC_{sat} and DIC_{dis}, and their separate responses to climate change (Fig. 10). The decrease of DIC_{dis} is mostly associated with the decrease in vertical mixing in high latitudes. Weaker vertical mixing and reduced deep and intermediate water formation imply that less DIC_{rem} is brought to the surface in a given amount of time, surface waters have now more time to equilibrate with the atmosphere, and that less of the surface DIC_{dis} penetrates to the deep via deep and intermediate waters . All three aspects contribute to the decreases of DIC_{dis} observed in Fig. 10.

The reverse is also true: enhanced vertical mixing increases the amount of DIC_{rem} that touches the surface and gets transformed into DIC_{pre} (thereby decreasing DIC_{rem} and increasing DIC_{pre} concentrations), but some of the new DIC_{pre} appearing at the surface is lost to the atmosphere before being transported to the ocean interior (thereby making the negative perturbation to DIC_{rem} larger than the positive perturbation to DIC_{pre}). Conversely, gas exchange does not affect DIC_{rem} by definition. As a result, anomalies in DIC_{rem} are conserved.

Considering the full effects of climate change (Climate*), the resulting decreases of solubility and disequilibrium

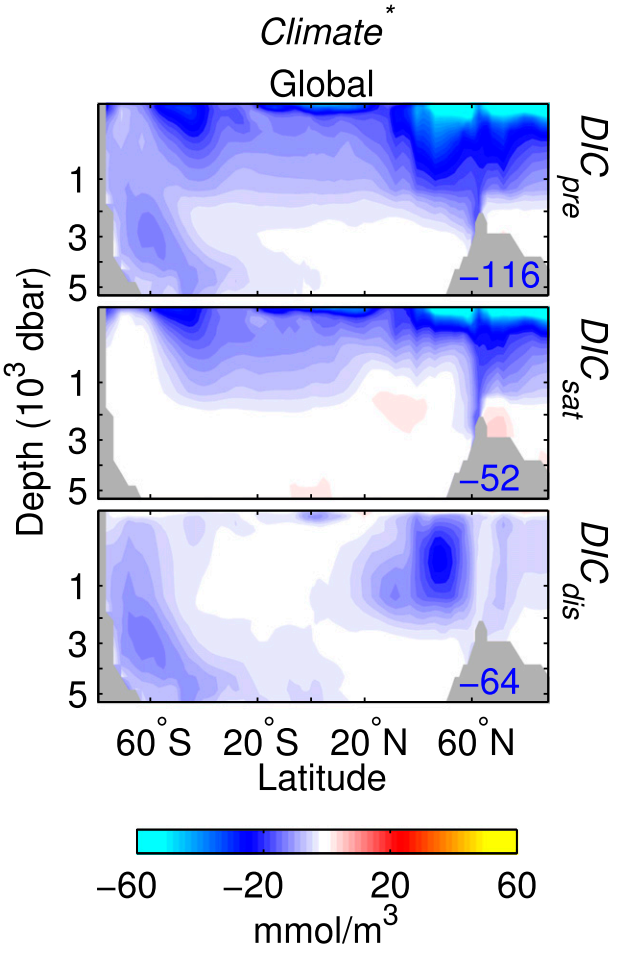

FIG. 10. Global zonal averages of DIC_{pre} and its two components DIC_{sat} and DIC_{dis}, as anomalies with respect to the preindustrial state in the Climate experiment. Numbers refer to total mass gained or lost (Pg C) for each DIC component. The figure shows the ensemble mean averaged over the period 2081–2100.

carbon dominate over the strengthening of the biological pump such that total DIC decreases (bottom panels in Fig. 5).

An interesting feature is present in the DIC_{sat} and DIC_{pre} response to climate change in the northern high latitudes. In the Gas_exchange experiment, the change in DIC_{pre} is primarily due to temperature and salinity driven changes in the DIC_{sat} component, with minimal change in DIC_{dis} (not shown). The patterns of DIC_{pre} in the Gas_exchange experiment (Fig. 5) and DIC_{sat} in the Climate experiment (Fig. 10) are then directly comparable, and very similar, suggesting that to a first order climate-driven changes in DIC_{sat} are driven by changes in SST and SSS affecting surface carbon solubility. However, a stronger decrease in DIC_{sat} in the Climate experiment in the northern high latitudes additionally reflects a climate-driven decrease in NADW formation rate and changes in surface Alk.

The final distribution of total oceanic DIC at the end of the twenty-first century in the Climate experiment reflects changes in the biological, chemical, and physical processes that regulate the uptake and storage of preformed and remineralized carbon. In a climate change scenario, DIC_{rem} increases in the deep and intermediate water formation regions at high latitudes but also everywhere in the deep ocean. While photosynthetic activity and remineralization occur to some degree everywhere, deep convection and the formation of the water masses that populate the deep ocean occur in very localized regions at high latitudes. Thus, the overall slowdown of the oceanic circulation allows for more DIC_{rem} to accumulate everywhere in the deep ocean due to continued, though weakening, global export production. Preformed DIC, on the other hand, relies solely on the circulation to reach the ocean interior, with no biological sources or sinks below the surface layer. For this reason the anomalies in deep ocean DIC_{pre} (mostly due to anomalies in DIC_{dis}) are tightly connected to the high latitudes, where deep and intermediate ventilation occurs. Importantly, DIC_{pre} is also affected by the surface solubility effect, which contributes to its overall decrease in concentration in the upper 1000 m, particularly in the subtropical cells and northern high latitudes (Fig. 10, middle panel). The integrated response to future climate change is a large redistribution of carbon in the ocean with a strengthened vertical DIC gradient at low latitudes and higher DIC concentrations at high latitudes (Fig. 5). This new distribution of DIC reflects the contribution (−20 Pg C) of the natural carbon cycle to the decrease of the total accumulated carbon uptake over the period 1860–2100 when climate-driven changes in the physical state of the ocean are taken into account.

e. *Sources of nonlinearity*

We have shown in section 3 that the wind stress perturbations (positive and negative) do not induce a strong feedback in the physical model. However, the sum of the DIC changes in the three perturbation experiments (Wind* + Buoyancy* + Gas_exchange*, final row of Fig. 6) do not sum precisely to the change in Climate*. This nonlinearity is most apparent for a single DIC reservoir (DIC_{pre} or DIC_{rem}) in a single basin. One example of a cause of such nonlinearity is the slowdown of convection, which can be brought on by both buoyancy forcing or wind stress perturbations, as is seen in the Weddell Sea. Convective mixing allows DIC_{rem} to reach the ocean's surface where some is outgassed and the rest converted to DIC_{pre}. Because convective mixing rapidly collapses in the Weddell Sea in Buoyancy* and slows considerably in Wind*, both accumulate DIC_{rem} there. However, the response of convection in Climate* in the

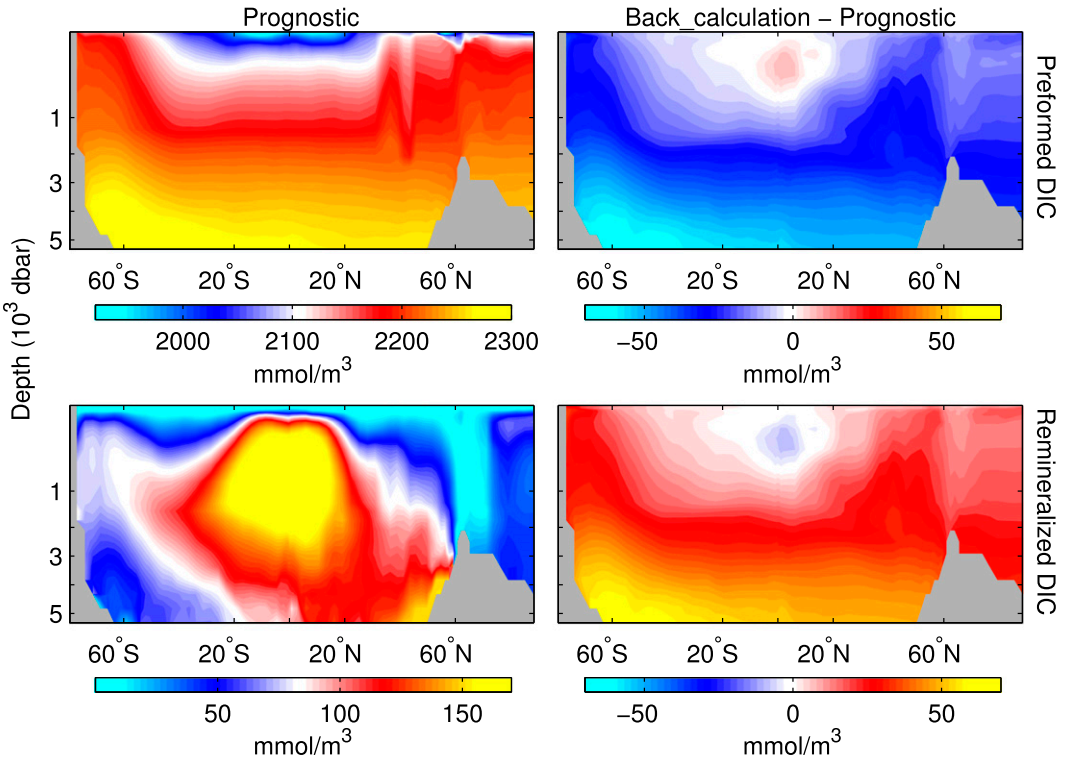

FIG. 11. Global zonal averages of DIC_{pre} and DIC_{rem} for the Control simulation as calculated with prognostic tracers (left column). The right column shows the difference between the estimate of DIC components using back-calculation techniques and the prognostic estimate. The figure shows the ensemble mean averaged over the period 2081–2100.

Weddell Sea does not significantly exceed its rapid shutdown in Buoyancy*. Thus the sum of Wind* and Buoyancy* in DIC_{rem} changes is larger than the corresponding change in Climate* in the Atlantic Ocean. Similar reasoning can be applied to the Gas_exchange experiment. Although this experiment does not have any effect on the circulation, the perturbation applied to the CO_2 gas exchange reflects climate-driven changes in heat and freshwater fluxes as well as associated changes in circulation. An anomaly in CO_2 solubility at the surface of the ocean is transported and diffused into the interior by a preindustrial circulation in this experiment. However, the perturbation applied reflects surface conditions in the Climate experiment where the same solubility anomaly is transported and diffused in a different way. This discrepancy represents another source of nonlinearity that prevents the sum of the carbon changes from the different physical perturbations to exactly equal the signal obtained from the Climate simulation.

f. Comparison with back-calculation estimates

To compare our method to separate DIC components with traditional back-calculation techniques we have also estimated DIC_{rem} using AOU and an empirical relationship for Alk_{pre} as it was done in previous modeling studies (e.g., Lauderdale et al. 2013; details are given in appendix B herein). Figure 11 shows the global zonal mean of DIC_{rem} and DIC_{pre} obtained with our method for the preindustrial simulation and the difference with the back-calculation method. As anticipated by Ito et al. (2004a) the use of AOU leads to an overestimate of the respiration (and of DIC_{rem}) in the deep ocean. In terms of total mass, Table 1 shows how DIC_{rem} estimated from AOU and empirical Alk_{pre} is about 26% higher than DIC_{rem} estimated with prognostic tracers. About 63% of this overestimation can be attributed to the DIC_{soft} portion of DIC_{rem} and is caused by the assumption of oxygen being in equilibrium everywhere at the ocean's surface. As shown by Ito et al. (2004a) and Duteil et al. (2013) this assumption is not valid at high latitudes because newly formed water masses remain undersaturated when they enter the ocean interior. The remaining 37% of the overestimation of DIC_{rem} is caused by the inherent error associated in the empirical relationship used for the calculation of Alk_{pre}. In addition to the differences for the total DIC_{rem} pool between the back-calculation

and prognostic methods in the Control simulation, the change in DIC_{rem} under anthropogenic climate forcing is also different between the two techniques. In the Climate simulation, the change in DIC_{rem} estimated with the back-calculation method is 24% lower than the change estimated with prognostic tracers (Table 1). While the qualitative nature of our results (e.g., enhanced storage of DIC_{rem} under climate change) would have been similar with either calculation technique, the quantitative differences are substantial: the back-calculation method underestimates the perturbation to DIC_{rem} and this bias is mostly due to the response of the DIC_{soft} portion. We hypothesize that this underestimation stems from the assumption that O_2 is saturated everywhere at the ocean's surface, which leads to an overestimate of baseline DIC_{rem}. As noted above, this assumption is most faulty in deep-water formation regions, where surface waters are significantly undersaturated. When deep-water formation slows, as is the case in the Climate simulation, there are fewer regions at the ocean's surface far from O_2 equilibrium. However, the back-calculation method misses this evolution of the surface O_2 disequilibrium and therefore underestimates the response of the DIC_{rem} pool under anthropogenic climate forcing. Although we have not archived a prognostic tracer for preformed oxygen we can still verify this explanation by quantifying the oxygen disequilibrium (ΔO_2) given the fixed stoichiometry assumed in the model (see appendix B for details). The difference in globally integrated ΔO_2 between the Climate and the Control simulations accounts for about 25 Pg C (after transforming it back to carbon) which equals almost exactly the difference in DIC_{rem} response to climate change forcing between the prognostic and back-calculation methods.

6. Conclusions

Our model results show that when changes in the physical state of the ocean are taken into account, climate change acts to modify the ocean natural carbon cycle contributing 20 Pg C to the decrease of the total accumulated carbon uptake over the period 1860–2100, under historical+RCP8.5 radiative forcing. This reduction in natural carbon storage represents a small positive feedback on atmospheric pCO_2. Importantly, this decrease in natural carbon storage is the residual between a significant strengthening in the storage of remineralized carbon (+96 Pg C) and an even larger reduction in preformed carbon (−116 Pg C). The enhanced remineralized carbon storage is due to the overall stratification of the water column resulting in reduced upwelling or mixing of carbon rich deep waters to the surface. The reduction in preformed carbon is to a similar extent due to warming-induced decreases in CO_2 solubility (and hence DIC_{sat}, −52 Pg C) and circulation-driven decreases in the amount of disequilibrium carbon penetrating in the deep ocean (DIC_{dis}, −64 Pg C). Our work shows that the magnitude of the redistribution of DIC in the ocean interior will depend strongly on the evolution of the ocean's overturning circulation over the twenty-first century, which depends in turn on wind and buoyancy changes. Although not directly addressed in our analysis, the preindustrial strength of natural carbon storage is likely to be another determining factor in setting the magnitude of oceanic carbon redistribution and the air–sea carbon partitioning under future climate change. Marinov et al. (2008a) showed, for example, that models with a highly efficient initial biological carbon pump respond less to factors that aim to increase the remineralized carbon storage.

Earth system models used to predict future climate trends (e.g., the CMIP5 model suite) show a wide range of MOC responses to a given emission scenario (Cheng et al. 2013) and use different parameterizations of oceanic biogeochemical processes; this will result in different background strengths of the biological pump and different degrees of redistribution and compensation between the biological and solubility driven processes over the twenty-first century. Our results suggest that changes in solubility and disequilibrium carbon are likely to dominate over changes in remineralized carbon. Separating the DIC into its various components helps to provide a mechanistic understanding of the ocean's response to a perturbation, which may be hidden when considering only the total DIC. Such a separation may help evaluate climate model skill against observational estimates of the partitioned DIC, as has been done for preformed and remineralized nutrients (Duteil et al. 2012). Moreover, a partitioning of the DIC components links DIC with other aspects of ocean biogeochemistry, with an important example provided by the consumption of oxygen implied in a shift from DIC_{pre} to DIC_{rem}. Further, we have shown how the use of prognostic tracers instead of back-calculation techniques for the DIC decomposition, reveals a more reactive DIC_{rem} pool, adding importance to the uncertainties associated to the formulation of biogeochemical models.

Two important caveats of our study are the use of a coarse-resolution model, and the simplified representation of ecological processes. The issue of model resolution on the response of ocean circulation to climate change and repercussions on carbon cycling are topics of active research in both modeling and observational communities (Hallberg and Gnanadesikan 2006; Farneti et al. 2010; Farneti and Delworth 2010; Ito et al. 2010; Meredith et al. 2012; Sallee et al. 2012; Dufour et al.

2012). There are many uncertainties in the degree to which an eddy-parameterizing model can faithfully simulate the ocean's response to perturbations in forcing. A well-known example of this uncertainty is in the Southern Ocean, where an increase and poleward shift in westerly wind stress has already been observed (Thompson and Solomon 2002). Coarse-resolution models typically show that such an increase should strengthen Southern Ocean upwelling and hence CO_2 outgassing (Lovenduski et al. 2008; Delworth and Zeng 2008; Le Quéré et al. 2010), while eddy-resolving models point to a largely reduced response due to compensating responses of eddy-driven and Eulerian mean flows (Farneti et al. 2010; Meredith et al. 2012). Some observational studies are in disagreement as to whether the upwelling and the ventilation rates have changed or not (Böning et al. 2008; Waugh et al. 2013).

While biological productivity in our model is allowed to vary with light, temperature, and nutrients, which change with climate change, the remineralization profile is parameterized with a Martin-type curve (Martin et al. 1987), which only depends on the variable oxygen concentrations. It is not yet clear how ecological processes not included in this model such as changes in organic matter stoichiometry and ecosystem composition (which might affect in turn the remineralization profile) will change over the twenty-first century. This uncertainty may turn out to be of similar importance to the uncertainty associated to eddy parameterization.

The response of the ocean carbon uptake to future climate change was studied in a previous generation of 3D coupled climate models with less sophisticated atmosphere–ocean physics and ocean biogeochemistry than our current model (Sarmiento and Le Quéré 1996; Sarmiento et al. 1998; Matear and Hirst 1999). It is interesting to see that despite the increasing sophistication in coupled physics and biogeochemistry, our results are qualitatively similar to results from those studies, where the authors also noticed large compensations between the biological effect and the circulation effect, with the direct effect of SST and SSS on carbon solubility decreasing the net oceanic carbon uptake. Our results suggest that reductions in surface CO_2 solubility will be the principal driver of the natural ocean carbon cycle response to climate warming over the twenty-first century. Contributions of the opposite sign will come from any weakening of the overturning circulation, mainly driven by changes in buoyancy fluxes, with wind-driven changes probably playing a minor role. However, we point out that, although these conclusions seem to hold up across subsequent generations of models, the high uncertainty associated with coarse resolution and biogeochemical parameterizations is still a major issue preventing us from safely excluding model dependency of these results.

Acknowledgments. RB, IM, and RS were sponsored by NOAA Grant NOAA-NA10OAR4310092. JBP was supported by the Natural Sciences and Engineering Research Council (NSERC). EG was supported by the Canadian Institute for Advanced Research (CIFAR) and NSERC. This work was partially supported by the Carbon Mitigation Initiative (CMI) project at Princeton University, sponsored by BP and Ford Motor Company. The authors want to thank Prof. Pierre Friedlingstein and three anonymous reviewers for their constructive comments on the manuscript and Anna Cabre for assistance with MLR calculations.

APPENDIX A

Biogeochemical Model Description

a. $CaCO_3$ production and dissolution

It has been argued that $CaCO_3$ production by plankton depends on temperature, carbonate saturation state, and overall growth rates. However, an analysis by Jin et al. (2006) suggests that the $CaCO_3$ production can be captured by scaling primary production by a constant rain ratio. We therefore follow the simple approach of a fixed Ca:P production ratio for small phytoplankton. The magnitude of this term is chosen to match the global $CaCO_3$ export flux estimate of Sarmiento et al. (2002) under preindustrial forcing. For the dissolution of $CaCO_3$ we calculate the carbonate saturation state ($CO_3^{2-}/CO_3^{2\text{-sat}}$) from DIC and Alk following Sayles (1985). This is then used to modify the default dissolution length scale of 1343 m, such that there is no dissolution of sinking carbonate at $CO_3^{2-} > CO_3^{2\text{-sat}}$, and the dissolution length scale decreases from infinity to 1343 m as CO_3^{2-} approaches zero. The $CaCO_3$ reaching the sediment is instantaneously dissolved and returned to the water column.

b. Organic carbon cycle, alkalinity, and gas exchange

Organic carbon cycles in a constant ratio with P (C:P = 106). This relationship holds through the uptake of PO_4, and the production and remnineralization of dissolved and sinking organic P. Biological productivity is allowed to vary with light, temperature, and nutrients [see Galbraith et al. (2010) for a detailed description], the production of sinking particles follows Dunne et al. (2005), and the remineralization profile is parameterized with a Martin-type curve (Martin et al. 1987), which depends on the variable oxygen concentrations. Alkalinity is a prognostic tracer. It is subject to transportation by ocean circulation, and to biogeochemical sources and sinks ($CaCO_3$ production and dissolution, and the implicit consumption and regeneration of NO_3). There are no external inputs or

outputs (i.e., the whole ocean alkalinity is conserved). Gas exchange is calculated with the Ocean–Carbon Cycle Model Intercomparison Project (OCMIP2) protocol (Najjar and Orr 1999) using the wind speed-dependent parameterization of Wanninkhof (1992).

APPENDIX B

Back-Calculation Technique for DIC Decomposition

Based on the ideas of Brewer (1978) and Chen and Millero (1979) we calculated first the oxygen saturation concentration (O_2^{sat}) as a function of temperature and salinity following Garcia and Gordon (1992). Assuming constant ratios $r_{O:P} = 150$ and $r_{C:P} = 106$ we calculated

$$DIC_{soft} = r_{C:P}/r_{O:P}(O_2^{sat} - O_2). \quad (B1)$$

To calculate the carbonate dissolution contribution to DIC we assumed surface salinity (S) and the tracer PO (Broecker 1974), defined as

$$PO = O_2 + r_{O:P}PO_4, \quad (B2)$$

as independent variables in a multiple linear regression with surface Alk as a dependent variable (Gruber et al. 1996). We use this relation to calculate Alk_{pre} everywhere in the ocean as

$$Alk_{pre} = 0.036 + (0.067S) + (0.102PO). \quad (B3)$$

We finally calculate DIC_{carb}, assuming $r_{N:P} = 16$ as

$$DIC_{carb} = 0.5[Alk - Alk_{pre} + (r_{N:P}/r_{O:P})(O_2^{sat} - O_2)]. \quad (B4)$$

Considered the fixed stoichiometry assumed in the model we can calculate preformed oxygen as

$$O_2^{pre} = r_{O:P}(PO_4 - PO_4^{pre}) + O_2 \quad (B5)$$

and oxygen disequilibrium as

$$\Delta O_2 = O_2^{pre} - O_2^{sat}. \quad (B6)$$

REFERENCES

Anderson, L. A., and J. L. Sarmiento, 1994: Redfield ratios of remineralization determined by nutrient data analysis. *Global Biogeochem. Cycles,* **8,** 65–80, doi:10.1029/93GB03318.

Arblaster, J. M., G. A. Meehl, and D. J. Karoly, 2011: Future climate change in the Southern Hemisphere: Competing effects of ozone and greenhouse gases. *Geophys. Res. Lett.,* **38,** L02701, doi:10.1029/2010GL045384.

Archer, D., P. Martin, B. Buffett, V. Brovkin, S. Rahmstorf, and A. Ganopolski, 2004: The importance of ocean temperature to global biogeochemistry. *Earth Planet. Sci. Lett.,* **222,** 333–348, doi:10.1016/j.epsl.2004.03.011.

Böning, C. W., A. Dispert, M. Visbeck, S. R. Rintoul, and F. U. Schwarzkopf, 2008: The response of the Antarctic Circumpolar Current to recent climate change. *Nat. Geosci.,* **1,** 864–869, doi:10.1038/ngeo362.

Brewer, P., 1978: Direct observation of oceanic CO_2 increase. *Geophys. Res. Lett.,* **5,** 997–1000, doi:10.1029/GL005i012p00997.

Broecker, W. S., 1974: ''NO,'' a conservative water-mass tracer. *Earth Planet. Sci. Lett.,* **23,** 100–107, doi:10.1016/0012-821X(74)90036-3.

Capotondi, A., M. A. Alexander, N. A. Bond, E. N. Curchitser, and J. D. Scott, 2012: Enhanced upper ocean stratification with climate change in the CMIP3 models. *J. Geophys. Res.,* **117,** C04031, doi:10.1029/2011JC007409.

Chen, G., and F. Millero, 1979: Gradual increase of oceanic CO_2. *Nature,* **277,** 205–206, doi:10.1038/277205a0.

Cheng, W., J. C. H. Chiang, and D. Zhang, 2013: Atlantic meridional overturning circulation (AMOC) in CMIP5 models: RCP and historical simulations. *J. Climate,* **26,** 7187–7197.

Cionni, I., and Coauthors, 2011: Ozone database in support of CMIP5 simulations: Results and corresponding radiative forcing. *Atmos. Chem. Phys.,* **11,** 11 267–11 292, doi:10.5194/acp-11-11267-2011.

de Lavergne, C., J. Palter, E. Galbraith, R. Bernardello, and I. Marinov, 2014: Cessation of deep convection in the open Southern Ocean under anthropogenic climate change. *Nat. Climate Change,* in press.

Delworth, T. L., and F. Zeng, 2008: Simulated impact of altered Southern Hemisphere winds on the Atlantic meridional overturning circulation. *Geophys. Res. Lett.,* **35,** L20708, doi:10.1029/2008GL035166.

Downes, S. M., and A. M. Hogg, 2013: Southern Ocean circulation and eddy compensation in CMIP5 models. *J. Climate,* **26,** 7198–7220.

Dufour, C. O., J. Le Sommer, J. D. Zika, M. Gehlen, J. C. Orr, P. Mathiot, and B. Barnier, 2012: Standing and transient eddies in the response of the Southern Ocean meridional overturning to the southern annular mode. *J. Climate,* **25,** 6958–6974.

Dunne, J. P., R. A. Armstrong, A. Gnanadesikan, and J. L. Sarmiento, 2005: Empirical and mechanistic models for the particle export ratio. *Global Biogeochem. Cycles,* **19,** GB4026, doi:10.1029/2004GB002390.

——, and Coauthors, 2012: GFDL's ESM2 global coupled climate–carbon earth system models. Part I: Physical formulation and baseline simulation characteristics. *J. Climate,* **25,** 6646–6665.

Durack, P. J., and S. E. Wijffels, 2010: Fifty-year trends in global ocean salinities and their relationship to broad-scale warming. *J. Climate,* **23,** 4342–4362.

Duteil, O., and Coauthors, 2012: Preformed and regenerated phosphate in ocean general circulation models: Can right total concentrations be wrong? *Biogeosciences,* **9,** 1797–1807, doi:10.5194/bg-9-1797-2012.

——, W. Koeve, A. Oschlies, D. Bianchi, I. Kriest, E. Galbraith, and R. Matear, 2013: A new estimate of ocean oxygen utilization points to a reduced rate of respiration in the ocean interior. *Biosci. Discuss.,* **10,** 2245–2267, doi:10.5194/bgd-10-2245-2013.

Farneti, R., and T. L. Delworth, 2010: The role of mesoscale eddies in the remote oceanic response to altered Southern Hemisphere winds. *J. Phys. Oceanogr.,* **40,** 2348–2354.

——, ——, A. J. Rosati, S. M. Griffies, and F. Zeng, 2010: The role of mesoscale eddies in the rectification of the Southern Ocean response to climate change. *J. Phys. Oceanogr.,* **40,** 1539–1557.

Follows, M., and R. Williams, 2004: Mechanisms controlling the air–sea flux of CO_2 in the North Atlantic. *The Ocean Carbon Cycle and Climate,* M. Follows and T. Oguz, Eds., Kluwer Academic, 217–249.

Galbraith, E. D., A. Gnanadesikan, J. P. Dunne, and M. R. Hiscock, 2010: Regional impacts of iron-light colimitation in a global biogeochemical model. *Biogeosciences,* **7,** 1043–1064.

——, and Coauthors, 2011: Climate variability and radiocarbon in the CM2Mc earth system model. *J. Climate,* **24,** 4230–4254.

Garcia, H. E., and L. I. Gordon, 1992: Oxygen solubility in seawater: Better fitting equations. *Limnol. Oceanogr.,* **37,** 1307–1312.

Gent, P. R., and J. C. McWilliams, 1990: Isopycnal mixing in ocean circulation models. *J. Phys. Oceanogr.,* **20,** 150–155.

Goodwin, P., and T. M. Lenton, 2009: Quantifying the feedback between ocean heating and CO_2 solubility as an equivalent carbon emission. *Geophys. Res. Lett.,* **36,** L15609, doi:10.1029/2009GL039247.

——, R. G. Williams, M. J. Follows, and S. Dutkiewicz, 2007: Ocean–atmosphere partitioning of anthropogenic carbon dioxide on centennial timescales. *Global Biogeochem. Cycles,* **21,** GB1014, doi:10.1029/2006GB002810.

Griffies, S. M., and Coauthors, 2005: Formulation of an ocean model for global climate simulations. *Ocean Sci.,* **1,** 45–79.

Gruber, N., and J. Sarmiento, 2002: Large-scale biogeochemical–physical interactions in elemental cycles. *Biological–Physical Interactions in the Sea,* A. R. Robinson, J. J. McCarthy, and B. J. Rothschild, Eds., *The Sea: Ideas and Observations on Progress in the Study of the Seas,* Vol. 12, John Wiley & Sons, 337–399.

——, ——, and T. Stocker, 1996: An improved method for detecting anthropogenic CO_2 in the oceans. *Global Biogeochem. Cycles,* **10,** 809–837, doi:10.1029/96GB01608.

Hallberg, R., and A. Gnanadesikan, 2006: The role of eddies in determining the structure and response of the wind-driven Southern Hemisphere overturning: Results from the Modeling Eddies in the Southern Ocean (MESO) project. *J. Phys. Oceanogr.,* **36,** 2232–2252.

Hirabara, M., H. Tsujino, H. Nakano, and G. Yamanaka, 2012: Formation mechanism of the Weddell Sea polynya and the impact on the global abyssal ocean. *J. Oceanogr.,* **68,** 771–796, doi:10.1007/s10872-012-0139-3.

Ito, T., and M. Follows, 2005: Preformed phosphate, soft tissue pump and atmospheric CO_2. *J. Mar. Res.,* **63,** 813–839, doi:10.1357/0022240054663231.

——, ——, and E. Boyle, 2004a: Is AOU a good measure of respiration in the oceans? *Geophys. Res. Lett.,* **31,** L17305, doi:10.1029/2004GL020900.

——, J. Marshall, and M. Follows, 2004b: What controls the uptake of transient tracers in the Southern Ocean? *Global Biogeochem. Cycles,* **18,** GB2021, doi:10.1029/2003GB002103.

——, M. Woloszyn, and M. Mazloff, 2010: Anthropogenic carbon dioxide transport in the Southern Ocean driven by Ekman flow. *Nature,* **463,** 80–83, doi:10.1038/nature08687.

Iudicone, D., K. B. Rodgers, I. Stendardo, O. Aumont, G. Madec, L. Bopp, O. Mangoni, and M. R. d'Alcala, 2011: Water masses as a unifying framework for understanding the Southern Ocean carbon cycle. *Biogeosciences,* **8,** 1031–1052, doi:10.5194/bg-8-1031-2011.

Jin, X., N. Gruber, J. P. Dunne, J. L. Sarmiento, and R. A. Armstrong, 2006: Diagnosing the contribution of phytoplankton functional groups to the production and export of particulate organic carbon, $CaCO_3$, and opal from global nutrient and alkalinity distributions. *Global Biogeochem. Cycles,* **20,** GB2015, doi:10.1029/2005GB002532.

Karpechko, A. Y., N. P. Gillett, L. J. Gray, and M. Dall'Amico, 2010: Influence of ozone recovery and greenhouse gas increases on Southern Hemisphere circulation. *J. Geophys. Res.,* **115,** D22117, doi:10.1029/2010JD014423.

Kwon, E. Y., J. L. Sarmiento, J. R. Toggweiler, and T. DeVries, 2011: The control of atmospheric pCO_2 by ocean ventilation change: The effect of the oceanic storage of biogenic carbon. *Global Biogeochem. Cycles,* **25,** GB3026, doi:10.1029/2011GB004059.

Lauderdale, J., A. Garabato, K. Oliver, M. Follows, and R. Williams, 2013: Wind-driven changes in Southern Ocean residual circulation, ocean carbon reservoirs and atmospheric CO_2. *Climate Dyn.,* **41,** 2145–2164, doi:10.1007/s00382-012-1650-3.

Law, R. M., R. J. Matear, and R. J. Francey, 2008: Comment on "Saturation of the Southern Ocean CO_2 sink due to recent climate change." *Science,* **319,** 570, doi:10.1126/science.1149077.

Lenton, A., and R. J. Matear, 2007: Role of the southern annular mode (SAM) in southern ocean CO_2 uptake. *Global Biogeochem. Cycles,* **21,** GB2016, doi:10.1029/2006GB002714.

——, and Coauthors, 2012: The observed evolution of oceanic pCO_2 and its drivers over the last two decades. *Global Biogeochem. Cycles,* **26,** GB2021, doi:10.1029/2011GB004095.

Le Quéré, C., and Coauthors, 2007: Saturation of the Southern Ocean CO_2 sink due to recent climate change. *Science,* **316,** 1735–1738, doi:10.1126/science.1136188.

——, T. Takahashi, E. T. Buitenhuis, C. Rödenbeck, and S. C. Sutherland, 2010: Impact of climate change and variability on the global oceanic sink of CO_2. *Global Biogeochem. Cycles,* **24,** GB4007, doi:10.1029/2009GB003599.

Lovenduski, N. S., N. Gruber, and S. C. Doney, 2008: Toward a mechanistic understanding of the decadal trends in the Southern Ocean carbon sink. *Global Biogeochem. Cycles,* **22,** GB3016, doi:10.1029/2007GB003139.

Marinov, I., A. Gnanadesikan, J. Toggweiler, and J. Sarmiento, 2006: The Southern Ocean biogeochemical divide. *Nature,* **441,** 964–967, doi:10.1038/nature04883.

——, M. Follows, A. Gnanadesikan, J. L. Sarmiento, and R. D. Slater, 2008a: How does ocean biology affect atmospheric pCO_2? Theory and models. *J. Geophys. Res.,* **113,** C07032, doi:10.1029/2007JC004598.

——, A. Gnanadesikan, J. L. Sarmiento, J. R. Toggweiler, M. Follows, and B. K. Mignone, 2008b: Impact of oceanic circulation on biological carbon storage in the ocean and atmospheric pCO_2. *Global Biogeochem. Cycles,* **22,** GB3007, doi:10.1029/2007GB002958.

Martin, J., G. Knauer, D. Karl, and W. Broenkow, 1987: VERTEX—Carbon cycling in the northeast Pacific. *Deep-Sea Res. I,* **34,** 267–285, doi:10.1016/0198-0149(87)90086-0.

Matear, R. J., and A. Hirst, 1999: Climate change feedback on the future oceanic CO_2 uptake. *Tellus,* **51B,** 722–733, doi:10.1034/j.1600-0889.1999.t01-1-00012.x.

——, and A. Lenton, 2008: Impact of historical climate change on the Southern Ocean carbon cycle. *J. Climate,* **21,** 5820–5834.

Meredith, M. P., A. C. N. Garabato, A. M. Hogg, and R. Farneti, 2012: Sensitivity of the overturning circulation in the Southern Ocean to decadal changes in wind forcing. *J. Climate,* **25,** 99–110.

Milly, P. C. D., and A. B. Shmakin, 2002: Global modeling of land water and energy balances. Part I: The land dynamics (LaD) model. *J. Hydrometeor.,* **3,** 283–299.

Najjar, R., and J. C. Orr, 1999: Biotic-HOWTO. Internal Ocean-Carbon Cycle Model Intercomparison Project (OCMIP) Rep., Laboratoire des Sciences du Climat et l'Environnement, CEA, 15 pp.

Palter, J. B., S. M. Griffies, B. L. Samuels, E. D. Galbraith, A. Gnanadesikan, and A. Klocker, 2014: The deep ocean buoyancy budget and its temporal variability. *J. Climate,* **27,** 551–573.

Polvani, L. M., M. Previdi, and C. Deser, 2011: Large cancellation, due to ozone recovery, of future Southern Hemisphere atmospheric circulation trends. *Geophys. Res. Lett.,* **38,** L04707, doi:10.1029/2011GL046712.

Rayner, D., and Coauthors, 2011: Monitoring the Atlantic meridional overturning circulation. *Deep-Sea Res. II,* **58,** 1744–1753, doi:10.1016/j.dsr2.2010.10.056.

Riahi, K., A. Gruebler, and N. Nakicenovic, 2007: Scenarios of long-term socio-economic and environmental development under climate stabilization. *Technol. Forecasting Soc. Change,* **74,** 887–935, doi:10.1016/j.techfore.2006.05.026.

Sabine, C., and Coauthors, 2004: The oceanic sink for anthropogenic CO_2. *Science,* **305,** 367–371, doi:10.1126/science.1097403.

Sallee, J.-B., R. J. Matear, S. R. Rintoul, and A. Lenton, 2012: Localized subduction of anthropogenic carbon dioxide in the Southern Hemisphere oceans. *Nat. Geosci.,* **5,** 579–584, doi:10.1038/NGEO1523.

Sarmiento, J., and J. Toggweiler, 1984: A new model for the role of the oceans in determining atmospheric pCO_2. *Nature,* **308,** 621–624, doi:10.1038/308621a0.

——, and C. Le Quéré, 1996: Oceanic carbon dioxide uptake in a model of century-scale global warming. *Science,* **274,** 1346–1350, doi:10.1126/science.274.5291.1346.

——, and N. Gruber, 2006: *Ocean Biogeochemical Dynamics.* Princeton University Press, 526 pp.

——, T. Hughes, R. Stouffer, and S. Manabe, 1998: Simulated response of the ocean carbon cycle to anthropogenic climate warming. *Nature,* **393,** 245–249, doi:10.1038/30455.

——, J. Dunne, A. Gnanadesikan, R. M. Key, K. Matsumoto, and R. Slater, 2002: A new estimate of the $CaCO_3$ to organic carbon export ratio. *Global Biogeochem. Cycles,* **16,** 1107, doi:10.1029/2002GB001919.

Sayles, F., 1985: $CaCo_3$ solubility in marine-sediments—Evidence for equilibrium and non-equilibrium behavior. *Geochim. Cosmochim. Acta,* **49,** 877–888, doi:10.1016/0016-7037(85)90180-2.

Sigman, D. M., and E. Boyle, 2000: Glacial/interglacial variations in atmospheric carbon dioxide. *Nature,* **407,** 859–869, doi:10.1038/35038000.

——, M. P. Hain, and G. H. Haug, 2010: The polar ocean and glacial cycles in atmospheric CO_2 concentration. *Nature,* **466,** 47–55, doi:10.1038/nature09149.

Simpkins, G. R., and A. Y. Karpechko, 2012: Sensitivity of the southern annular mode to greenhouse gas emission scenarios. *Climate Dyn.,* **38,** 563–572, doi:10.1007/s00382-011-1121-2.

Son, S.-W., N. F. Tandon, L. M. Polvani, and D. W. Waugh, 2009: Ozone hole and Southern Hemisphere climate change. *Geophys. Res. Lett.,* **36,** L15705, doi:10.1029/2009GL038671.

Strong, C., and R. E. Davis, 2007: Winter jet stream trends over the Northern Hemisphere. *Quart. J. Roy. Meteor. Soc.,* **133,** 2109–2115, doi:10.1002/qj.171.

Thompson, D., and S. Solomon, 2002: Interpretation of recent Southern Hemisphere climate change. *Science,* **296,** 895–899, doi:10.1126/science.1069270.

Volk, T., and M. I. Hoffert, 1985: Ocean carbon pumps: Analysis of relative strengths and efficiencies in ocean-driven atmospheric CO_2 changes. *The Carbon Cycle and Atmospheric CO_2: Natural Variations Archean to Present, Geophys. Monogr.,* Vol. 32, Amer. Geophys. Union, 99–110.

Wanninkhof, R., 1992: Relationship between wind speed and gas exchange over the ocean. *J. Geophys. Res.,* **97** (C5), 7373–7382.

Waugh, D. W., F. Primeau, T. DeVries, and M. Holzer, 2013: Recent changes in the ventilation of the southern oceans. *Science,* **339,** 568–570, doi:10.1126/science.1225411.

Wetzel, P., A. Winguth, and E. Maier-Reimer, 2005: Sea-to-air CO_2 flux from 1948 to 2003: A model study. *Global Biogeochem. Cycles,* **19,** GB2005, doi:10.1029/2004GB002339.

Williams, R., and M. Follows, 2011: *Ocean Dynamics and the Carbon Cycle: Principles and Mechanisms.* Cambridge University Press, 404 pp.

Zickfeld, K., J. C. Fyfe, M. Eby, and A. J. Weaver, 2008: Comment on "Saturation of the Southern Ocean CO_2 sink due to recent climate change." *Science,* **319,** 570, doi:10.1126/science.1146886.